

## SUPPORTING INFORMATION

### DISCOVERY OF NOVEL ACRA-B-TOLC PUMP INHIBITOR BY MULTISTEP VIRTUAL SCREENING, SYNTHESIS AND BIOLOGICAL EVALUATION OF ASYMMETRIC IMIDAZOLE-4,5-DICARBOXAMIDE DERIVATIVES†

Thien-Vy Phan,<sup>‡ab</sup> Phuong Nguyen Hoai Huynh,<sup>‡a</sup> Vu-Thuy-Vy Nguyen,<sup>ab</sup> Thanh-Phuc Nguyen,<sup>a</sup> Thanh-Thao Vu,<sup>a</sup> Cam-Van Thi Vo,<sup>a</sup> Minh-Tri Le,<sup>ac</sup> Bao Gia Dang Nguyen,<sup>d</sup> Phuong Truong,<sup>a</sup> and Khac-Minh Thai<sup>\*a</sup>

---

<sup>a.</sup> *Faculty of Pharmacy, University of Medicine and Pharmacy at Ho Chi Minh city, 41 Dinh Tien Hoang St., Dist. 1, Ho Chi Minh City 700000, Vietnam.*

*E-mail: [thaikhacminh@ump.edu.vn](mailto:thaikhacminh@ump.edu.vn)*

<sup>b.</sup> *Department of Pharmacy, Nguyen Tat Thanh University, 300A Nguyen Tat Thanh St., Dist. 4, Ho Chi Minh City 700000, Vietnam.*

<sup>c.</sup> *School of Medicine, Vietnam National University Ho Chi Minh City, Linh Trung Ward., Thu Duc Dist, Ho Chi Minh City, 700000, Vietnam.*

<sup>d.</sup> *Imperial College London, London SW7 2AZ, UK*

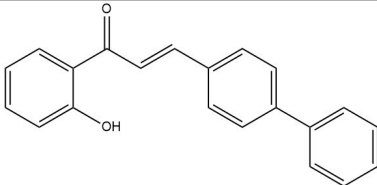
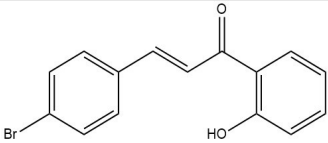
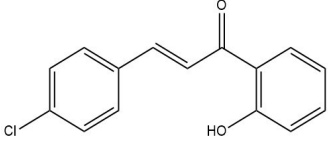
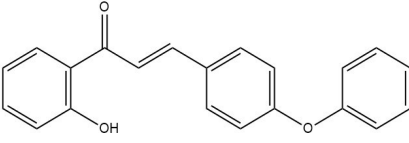
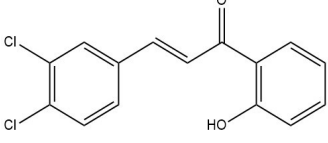
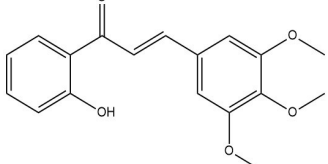
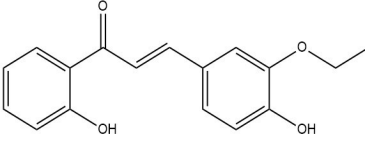
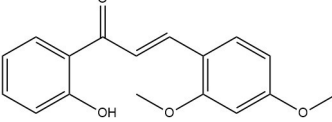
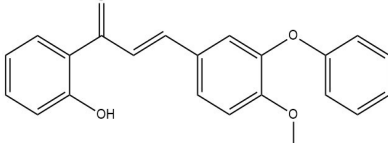
†Electronic Supplementary Information (ESI) available: See DOI: 10.1039/x0xx00000x

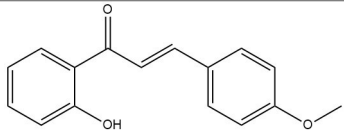
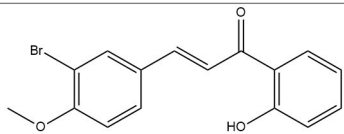
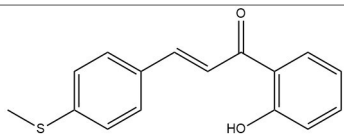
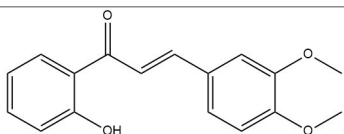
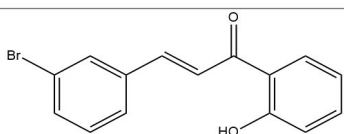
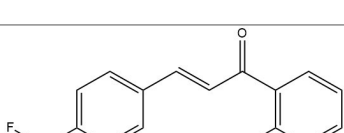
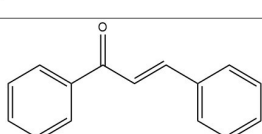
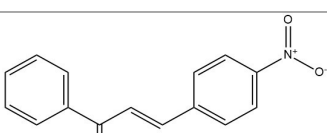
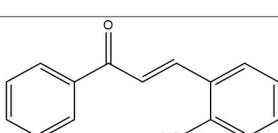
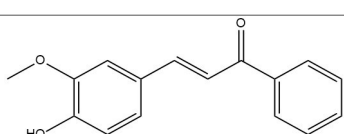
‡These authors contributed equally to this work and are co-first authors.

## Contents

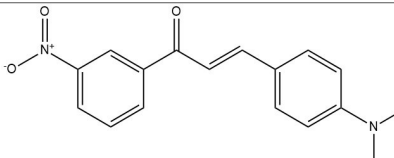
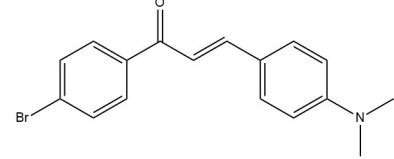
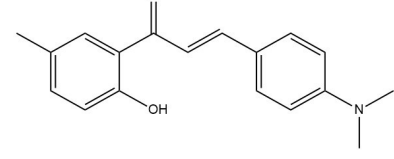
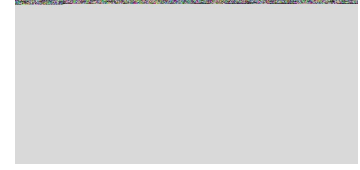
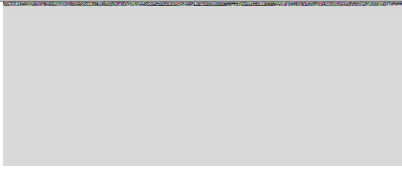
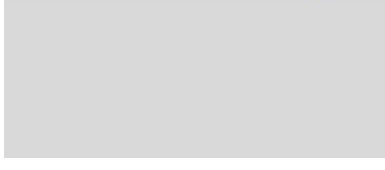
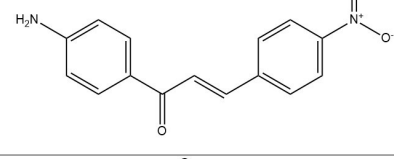
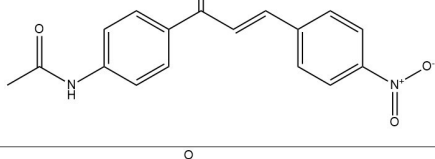
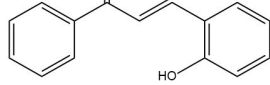
Table S1. The in-house database.....	1
Table S2. The result of screening <i>in silico</i> for the in-house database .....	32
Table S3. The interaction analysis of four compound's docking poses at distal pocket AcrB .....	34
Table S4. The number and occupancy of hydrogen bonds of A4 were calculated using the data of 100 ns simulations trajectory .....	34
Table S5. The relative potential of A1-4 to reduce the MIC of LEV and OXA against <i>E. coli</i> BW25113 ....	34
Figure S2. (A) Protein carbon backbone RMSD; (B) Radius of gyration; (C) Solvent accessible surface area and (D) Heavy-atom RMSD values of A4 calculated using the data of trajectories of 100 ns MD simulations .....	36
Figure S3. Carbon alpha RMSF values of the AcrB in apoprotein (orange) and in complex A4-AcrB (blue) were calculated using the data of 100 ns trajectories of MD simulations .....	36
Figure S4. Principal component analysis. (A) 2D projection of apoprotein (orange) and A4-AcrB (blue) calculated after 100 ns of MD trajectories. (B) EV1 collective motions in porcupine plot for apoprotein and A4-AcrB .....	37
Figure S6. MM/GBSA binding free energy variation over time of the complex is calculated using the trajectories of 100 ns MD simulations.....	37
Figure S7. Effects of four compounds at 100 $\mu$ M on accumulation of the fluorescent DNA-binding dye H33342, an AcrAB efflux pump substrate, in <i>E. coli</i> BW25113 .....	38
Figure S8. The A4's ADMET result generated from the ADMETlab2.0 server analyses.....	39
Experimental.....	40
The NMR Assignments, Infrared Spectroscopy and Mass Spectrum of synthetic compounds.....	49

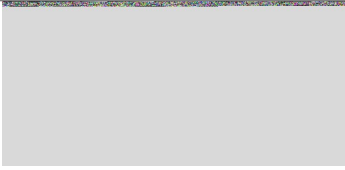
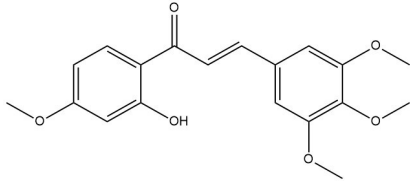
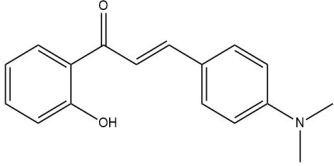
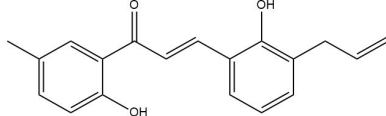
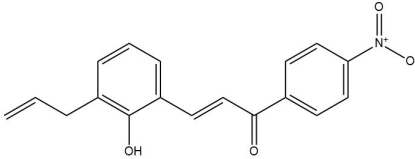
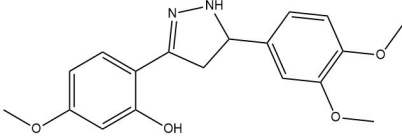
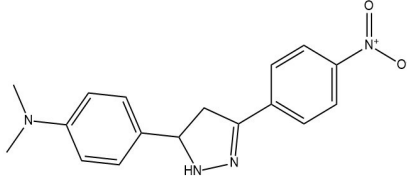
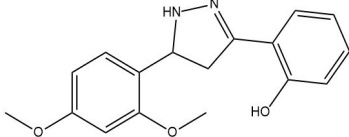
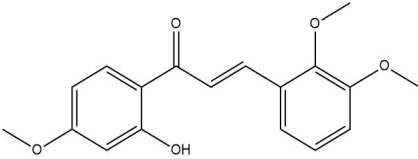
**Table S1.** The in-house database

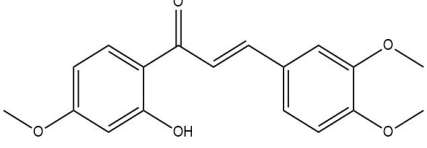
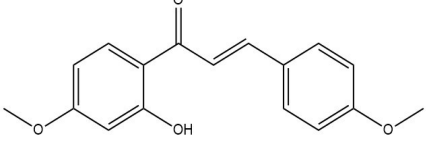
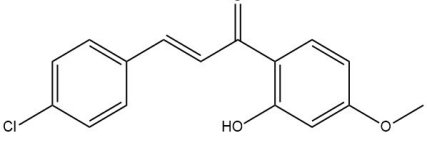
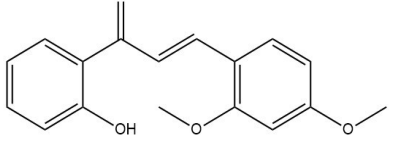
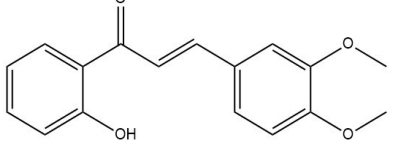
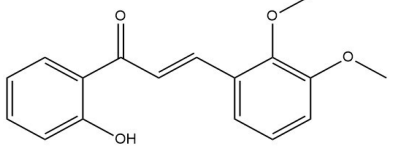
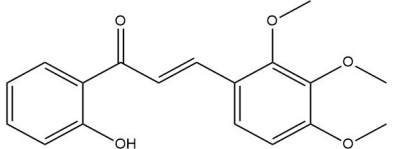
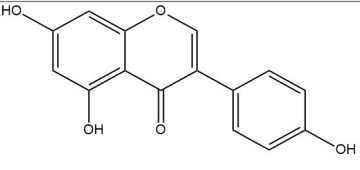
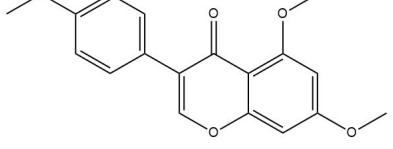
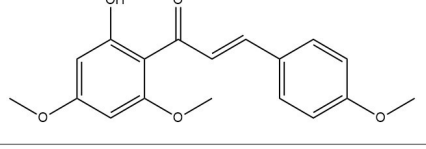
No.	Name	Structure
1.	2005_NTTV_SP1	
2.	2005_NTTV_SP11	
3.	2005_NTTV_SP12	
4.	2005_NTTV_SP13	
5.	2005_NTTV_SP14	
6.	2005_NTTV_SP15	
7.	2005_NTTV_SP16	
8.	2005_NTTV_SP17	
9.	2005_NTTV_SP18	

10.	2005_NTTV_SP2	
11.	2005_NTTV_SP3	
12.	2005_NTTV_SP4	
13.	2005_NTTV_SP5	
14.	2005_NTTV_SP8	
15.	2005_NTTV_SP9	
16.	2007_PNYV_N1	
17.	2007_PNYV_N2	
18.	2007_PNYV_N3	
19.	2007_PNYV_N4	

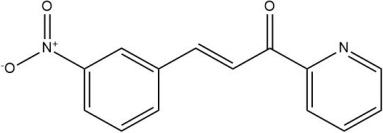
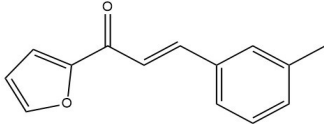
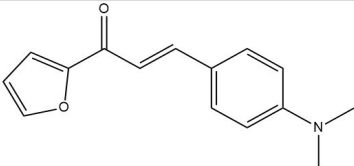
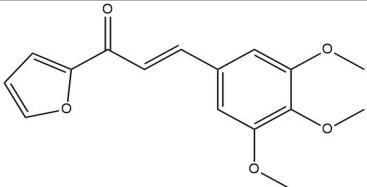
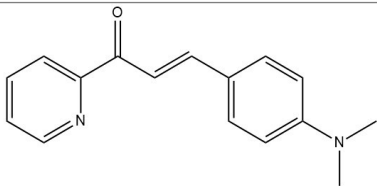
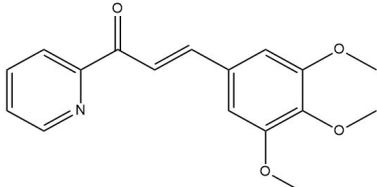
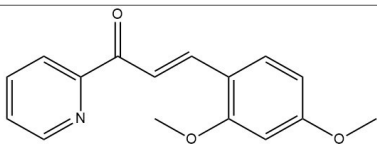
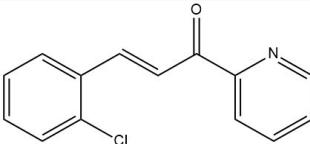
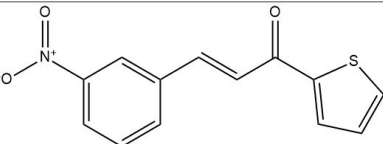
20.	2007_PNYV_N5	
21.	2007_PNYV_N6	
22.	2007_PNYV_N7	
23.	2007_PNYV_N8	
24.	2007_PNYV_N9	
25.	2007_PTPT_F1	
26.	2007_PTPT_F10	
27.	2007_PTPT_F11	
28.	2007_PTPT_F12	

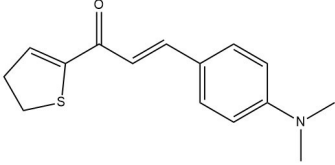
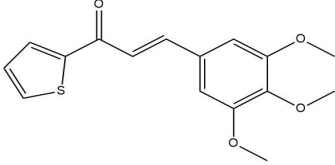
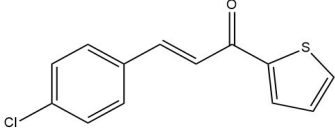
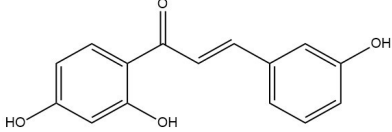
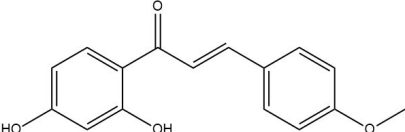
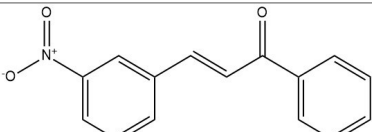
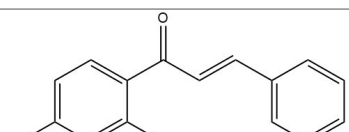
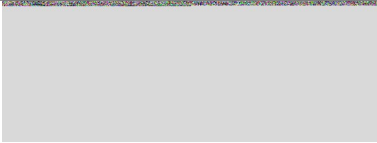
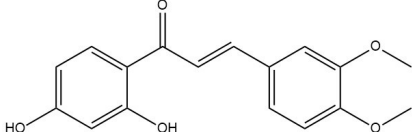
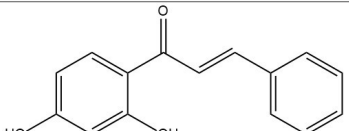
29.	2007_PTPT_F13	
30.	2007_PTPT_F14	
31.	2007_PTPT_F15	
32.	2007_PTPT_F2	
33.	2007_PTPT_F3	
34.	2007_PTPT_F4	
35.	2007_PTPT_F6	
36.	2007_PTPT_F7	
37.	2007_PTPT_F8	

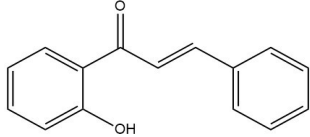

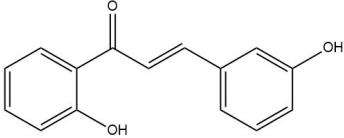
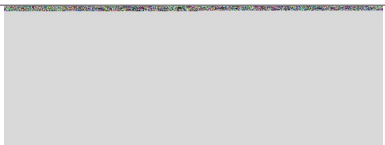
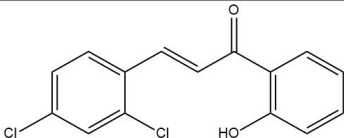
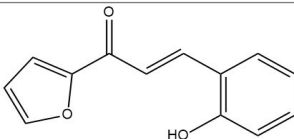
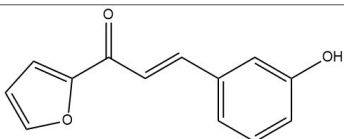
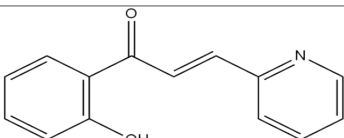
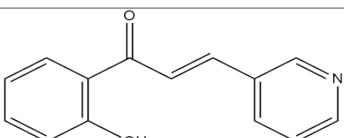
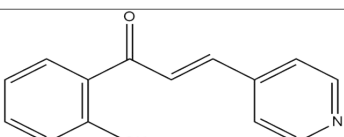
38.	2007_PTPT_F9	
39.	2008_DNT_T1	
40.	2008_DNT_T10	
41.	2008_DNT_T11	
42.	2008_DNT_T12	
43.	2008_DNT_T13	
44.	2008_DNT_T14	
45.	2008_DNT_T15	
46.	2008_DNT_T2	

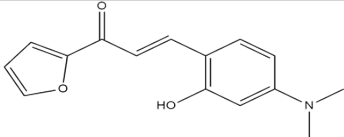
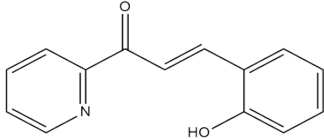
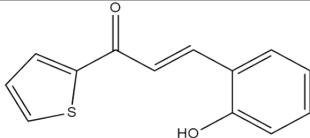
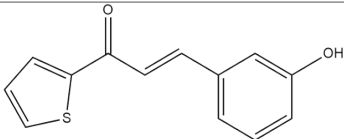
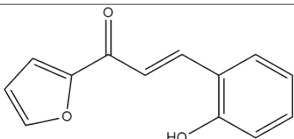
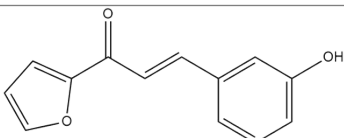
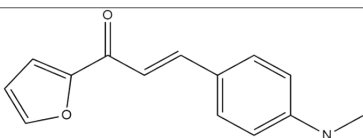
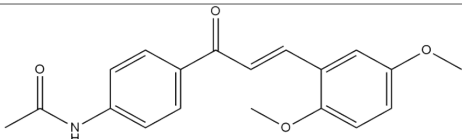
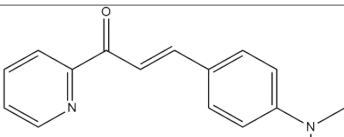
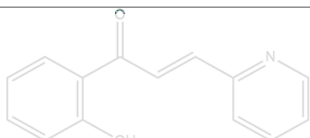
47.	2008_DNT_T3	
48.	2008_DNT_T4	
49.	2008_DNT_T5	
50.	2008_DNT_T6	
51.	2008_DNT_T7	
52.	2008_DNT_T8	
53.	2008_DNT_T9	
54.	2009_HKD_Genistein	
55.	2009_HKD_IsoflavonIII	
56.	2009_HKD_chalconII	

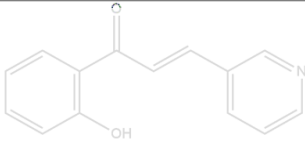
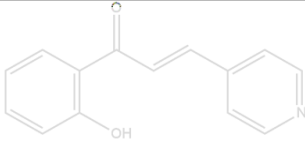
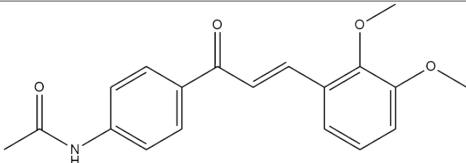
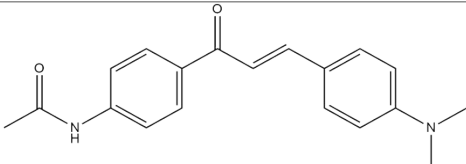
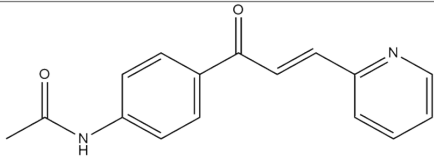
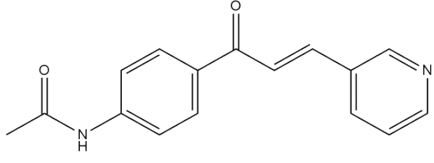
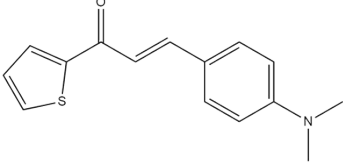
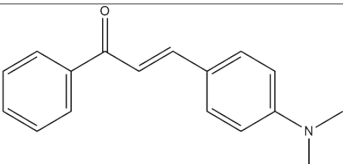
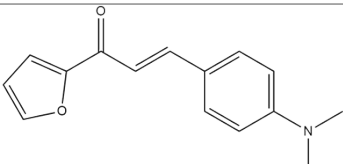


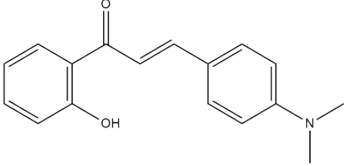
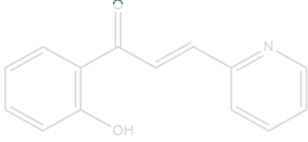
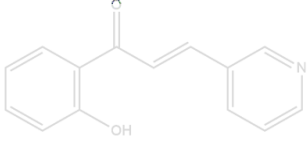
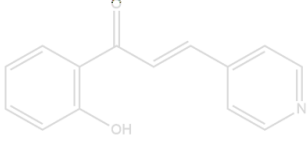
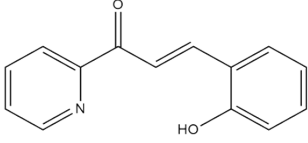
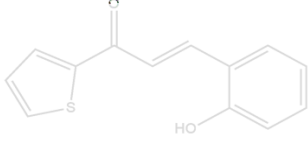
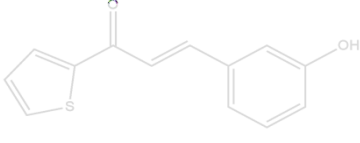
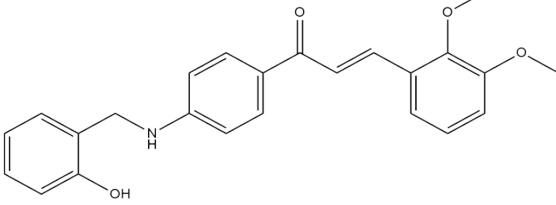
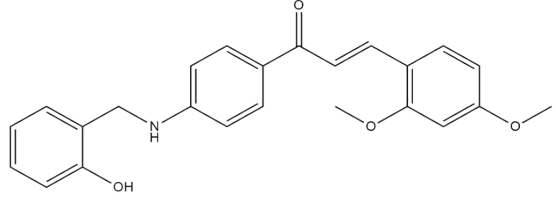
57.	2009_NTTN_N1	
58.	2009_NTTN_N10	
59.	2009_NTTN_N11	
60.	2009_NTTN_N12	
61.	2009_NTTN_N2	
62.	2009_NTTN_N3	
63.	2009_NTTN_N4	
64.	2009_NTTN_N5	
65.	2009_NTTN_N6	

66.	2009_NTTN_N7	
67.	2009_NTTN_N8	
68.	2009_NTTN_N9	
69.	2012_NHA_S15	
70.	2012_NHA_S19	
71.	2012_NHA_S25	
72.	2012_NHA_S3	
73.	2012_NHA_S42	
74.	2012_NHA_S43	
75.	2012_NTTH_H18	

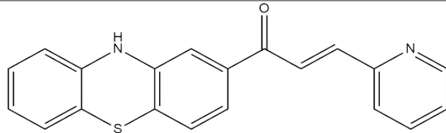
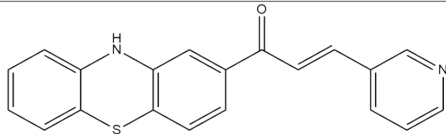
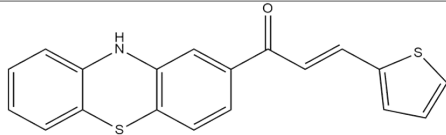
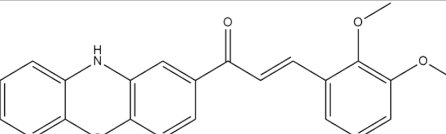
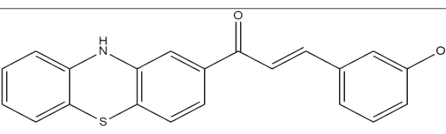
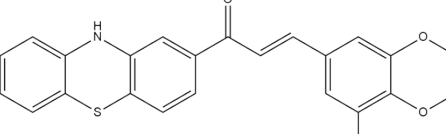
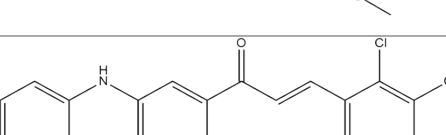
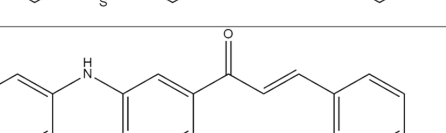
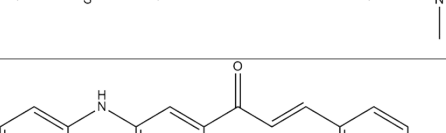
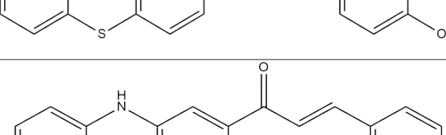
76.	2012_NTTH_H24	
77.	2012_NTTH_H5	
78.	2012_NTTH_H6	
79.	2012_NTTH_H7	
80.	2012_NTTH_H8	
81.	2013_LAT_F1	
82.	2013_LAT_F2	
83.	2013_LAT_H1	
84.	2013_LAT_H2	
85.	2013_LAT_H3	

86.	2013_LAT_N11	
87.	2013_LAT_P1	
88.	2013_LAT_T1	
89.	2013_LAT_T2	
90.	2013_NGU_FH2	
91.	2013_NGU_FH3	
92.	2013_NGU_FN4	
93.	2013_NGU_G1	
94.	2013_NGU_G10	
95.	2013_NGU_G11	

96.	2013_NGU_G12	
97.	2013_NGU_G13	
98.	2013_NGU_G2	
99.	2013_NGU_G3	
100.	2013_NGU_G4	
101.	2013_NGU_G5	
102.	2013_NGU_G6	
103.	2013_NGU_G7	
104.	2013_NGU_G8	

105.	2013_NGU_G9	
106.	2013_NGU_HP2	
107.	2013_NGU_HP3	
108.	2013_NGU_HP4	
109.	2013_NGU_PH2	
110.	2013_NGU_TH2	
111.	2013_NGU_TH3	
112.	2014_NGU_A23M	
113.	2014_NGU_A24M	

114.	2014_NGU_A2C	
115.	2014_NGU_A2F	
116.	2014_NGU_A2P	
117.	2014_NGU_A34M	
118.	2014_NGU_A4C	
119.	2014_NGU_A4N	
120.	2014_NGU_A4P	
121.	2014_NGU_AB	

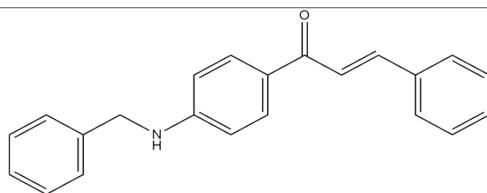
122.	2014_PHA_AP1	
123.	2014_PHA_AP2	
124.	2014_PHA_AP3	
125.	2014_PHA_AP4	
126.	2014_PHA_AP5	
127.	2014_PHA_AP6	
128.	2014_PHA_AP7	
129.	2014_PHA_AP8	
130.	2015_DON_AP1	
131.	2015_DON_AP10	



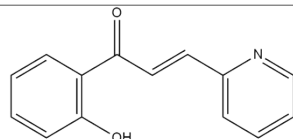
132.	2015_DON_AP2	
133.	2015_DON_AP3	
134.	2015_DON_AP4	
135.	2015_DON_AP5	
136.	2015_DON_AP6	
137.	2015_DON_AP7	
138.	2015_DON_AP8	
139.	2015_DON_AP9	
140.	2015_NGU_CS3	
141.	2015_NGU_FME	

142.	2015_NGU_HCP2	
143.	2015_NGU_HCP3	
144.	2015_NGU_PME	
145.	2015_NGU_TME	
146.	2015_TRA_A23M	
147.	2015_TRA_A24M	
148.	2015_TRA_A2C	
149.	2015_TRA_A3C	
150.	2015_TRA_A4C	

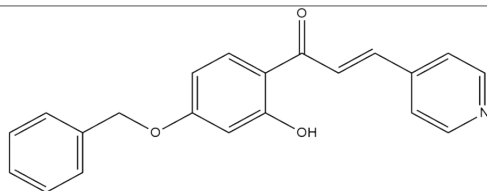
151. 2015\_TRA\_AB



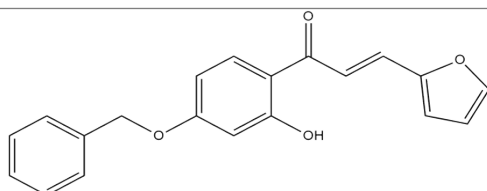
152. 2016\_VOD\_V1



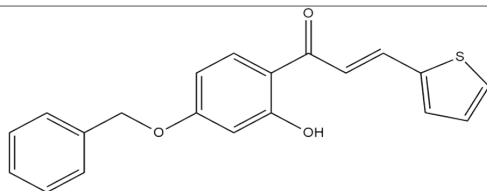
153. 2016\_VOD\_V10



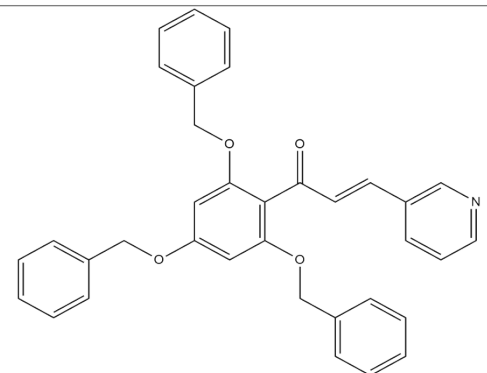
154. 2016\_VOD\_V11



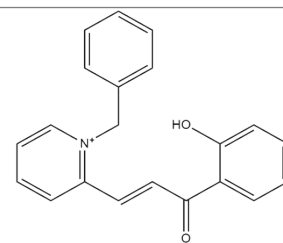
155. 2016\_VOD\_V12



156. 2016\_VOD\_V13



157. 2016\_VOD\_V14



158.	2016_VOD_V15	
159.	2016_VOD_V16	
160.	2016_VOD_V17	
161.	2016_VOD_V18	
162.	2016_VOD_V19	
163.	2016_VOD_V2	
164.	2016_VOD_V20	
165.	2016_VOD_V21	
166.	2016_VOD_V22	

167.	2016_VOD_V23	
168.	2016_VOD_V3	
169.	2016_VOD_V4	
170.	2016_VOD_V5	
171.	2016_VOD_V6	
172.	2016_VOD_V7	
173.	2016_VOD_V8	
174.	2016_VOD_V9	
175.	2016_VUH_T100	

176.	2016_VUH_T101	
177.	2016_VUH_T102	
178.	2016_VUH_T42	
179.	2016_VUH_T43	
180.	2016_VUH_T45	
181.	2016_VUH_T48	
182.	2016_VUH_T76	
183.	2016_VUH_T78	

184.	2016_VUH_T95	
185.	2016_VUH_T96	
186.	2016_VUH_T97	
187.	2016_VUH_T98	
188.	2016_VUH_T99	
189.	2017_NGU_C1	
190.	2017_NGU_C10	

191.	2017_NGU_C11	
192.	2017_NGU_C12	
193.	2017_NGU_C13	
194.	2017_NGU_C2	
195.	2017_NGU_C3	
196.	2017_NGU_C4	
197.	2017_NGU_C5	



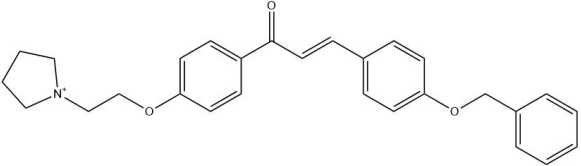
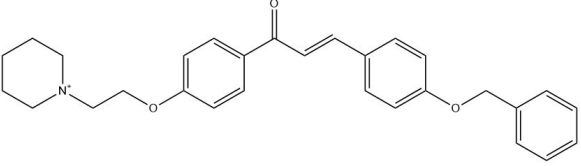
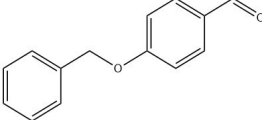
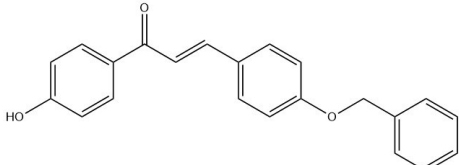
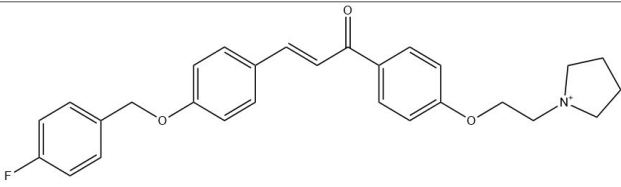
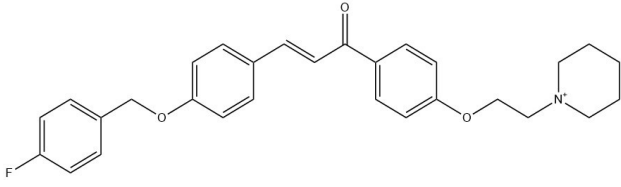
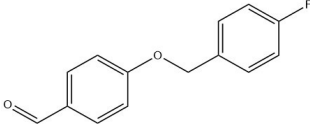
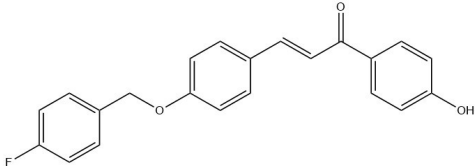
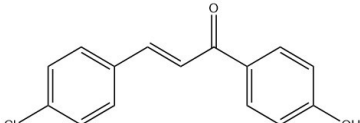
198.	2017_NGU_C6	
199.	2017_NGU_C7	
200.	2017_NGU_C8	
201.	2017_NGU_C9	
202.	2018_LTAT_C1	
203.	2018_LTAT_C2	
204.	2018_LTAT_C3	

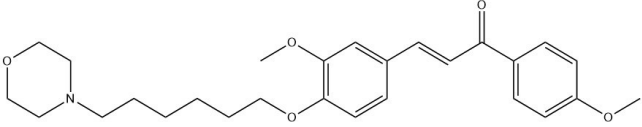
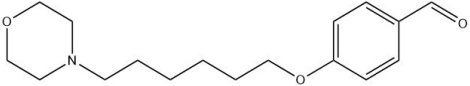
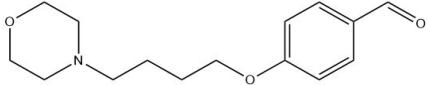
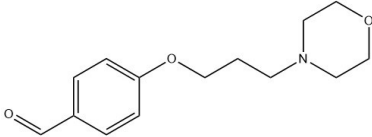
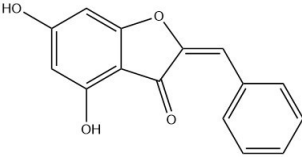
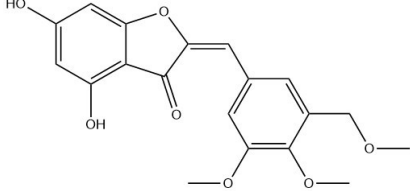
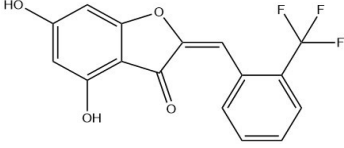
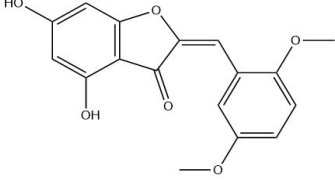
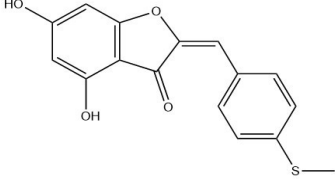
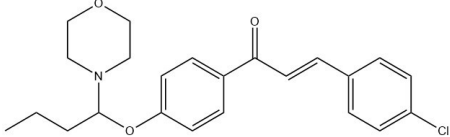
205.	2018_LTAT_C4	
206.	2018_LTAT_C5	
207.	2018_LTAT_C6	
208.	2018_LTAT_C7	
209.	2018_LTAT_C8	
210.	2018_LTAT_C9	
211.	2018_NHD_C1	
212.	2018_NHD_C2	
213.	2018_NHD_C3	

214.	2018_NHD_C4	
215.	2018_NHD_HC1	
216.	2018_NHD_HC2	
217.	2018_NHD_HC3	
218.	2018_NHD_HC4	
219.	2018_NHD_HT5	
220.	2018_NHD_HT6	

221.	2018_NHD_T5	
222.	2018_NHD_T6	
223.	2018_NHM_25	
224.	2018_NHM_B	
225.	2018_NHM_B2	
226.	2018_NHM_C	
227.	2018_NHM_C2	
228.	2018_NHM_C3	

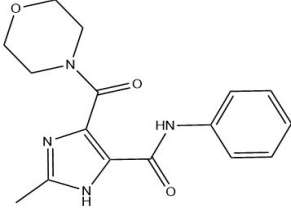
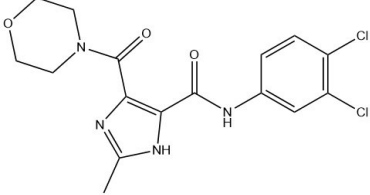
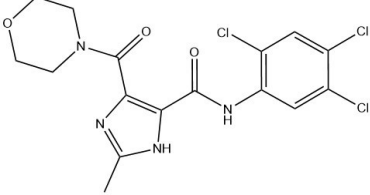
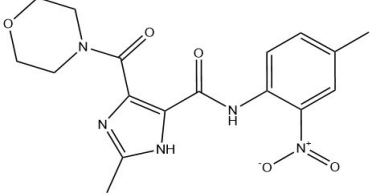
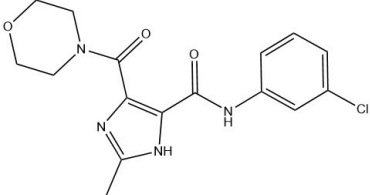
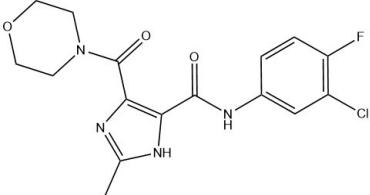
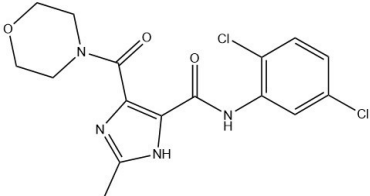
229.	2018_NHM_CF	
230.	2018_NHM_P3	
231.	2018_NHM_P4	
232.	2018_VDD_A5	
233.	2018_VDD_AC	
234.	2018_VDD_B5	
235.	2018_VDD_B6	
236.	2018_VDD_C5	
237.	2018_VDD_C6	
238.	2018_VDD_CC	

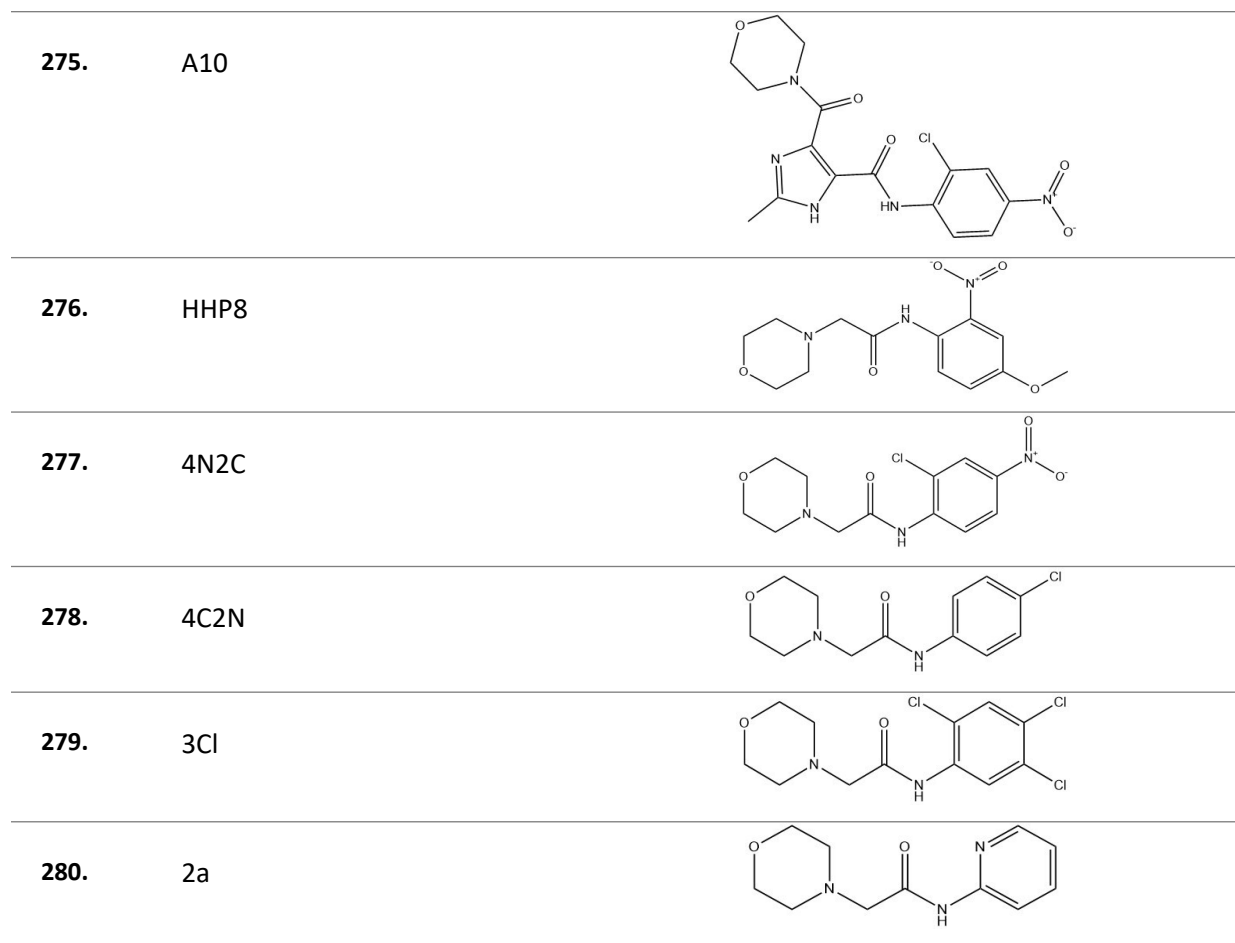
239.	2018_VDD_D5	
240.	2018_VDD_D6	
241.	2018_VDD_DA	
242.	2018_VDD_DC	
243.	2018_VDD_E5	
244.	2018_VDD_E6	
245.	2018_VDD_EA	
246.	2018_VDD_EC	
247.	Chalcon_2942_BC	

248.	TD6MC	
249.	TD6M	
250.	TD4M	
251.	TD3M	
252.	d9	
253.	D6	
254.	D5	
255.	D4	
256.	D3	
257.	C4.4	

258.	C4.1	
259.	C3.5	
260.	C3.4	
261.	C3.2	
262.	C3.1	
263.	C3.6	
264.	AH6M	
265.	AH4M	
266.	AH3M	
267.	A2	



268.	A1	
269.	A3	
270.	A4	
271.	A6	
272.	A7	
273.	A8	
274.	A11	



**Table S2.** The result of screening *in silico* for the in-house database

No.	Compound	Docking score (kJ.mol <sup>-1</sup> )	No.	Compound	Docking score (kJ.mol <sup>-1</sup> )
1.	2007_PTPT_F13	-26.00	18.	2018_NHM_25	-21.94
2.	2013_LAT_N11	-25.17	19.	2018_NHM_C	-21.84
3.	2016_VUH_T99	-24.61	20.	2008_DNT_T10	-21.68
4.	2013_NGU_G5	-24.04	21.	2013_NGU_G9	-21.68
5.	2016_VOD_V22	-23.61	22.	2016_VUH_T98	-21.57
6.	2014_NGU_A2C	-23.39	23.	2018_NHM_B2	-21.44
7.	2014_NGU_A23M	-23.20	24.	2016_VUH_T96	-21.35
8.	2014_NGU_A2P	-23.13	25.	2008_DNT_T9	-21.25
9.	2018_NHM_C3	-23.13	26.	2016_VOD_V13	-21.24
10.	2007_PTPT_F12	-23.01	27.	2008_DNT_T1	-21.18
11.	2015_TRA_A23M	-22.99	28.	2016_VOD_V10	-21.12
12.	2018_NHM_P3	-22.75	29.	2018_LTAT_C5	-21.07
13.	A3	-22.73	30.	2018_NHM_C2	-20.97
14.	2014_NGU_A24M	-22.67	31.	2014_NGU_A4N	-20.84
15.	2013_NGU_G3	-22.48	32.	2016_VUH_T45	-20.84
16.	2016_VOD_V9	-21.95	33.	2016_VUH_T95	-20.84
17.	2016_VUH_T48	-21.95	34.	2016_VOD_V8	-20.79

No.	Compound	Docking score (kJ.mol <sup>-1</sup> )
35.	A2	-20.77
36.	2015_TRA_A3C	-20.73
37.	2016_VUH_T43	-20.64
38.	2014_NGU_A4C	-20.63
39.	2014_NGU_AB	-20.63
40.	2016_VUH_T42	-20.63
41.	2015_TRA_A2C	-20.52
42.	2013_NGU_FN4	-20.47
43.	A4	-20.35
44.	2018_NHM_P4	-20.31
45.	2016_VUH_T97	-20.30
46.	A1	-20.27
47.	2015_TRA_A4C	-20.26
48.	2014_PHA_AP8	-20.18
49.	2016_VUH_T78	-20.17
50.	2015_DON_AP9	-20.14
51.	2018_LTAT_C9	-20.11
52.	2005_NTTV_SP3	-20.09
53.	2015_DON_AP7	-20.08
54.	2015_DON_AP8	-20.05
55.	2009_NTTN_N11	-20.04
56.	2013_NGU_G8	-20.04
57.	2014_NGU_A34M	-19.94
58.	2016_VOD_V12	-19.92
59.	2016_VOD_V11	-19.83
60.	2018_VDD_DC	-19.76
61.	2008_DNT_T14	-19.71
62.	2005_NTTV_SP15	-19.70
63.	2007_PTPT_F15	-19.68
64.	HHP8	-19.63
65.	2018_NHM_B	-19.58
66.	2014_NGU_A4P	-19.57
67.	2005_NTTV_SP14	-19.45
68.	2014_PHA_AP5	-19.44
69.	2012_NHA_S43	-19.43
70.	2009_NTTN_N2	-19.39
71.	2013_NGU_G10	-19.38
72.	2015_TRA_AB	-19.37
73.	2018_VDD_EC	-19.33
74.	2014_PHA_AP6	-19.31
75.	2005_NTTV_SP5	-19.23
76.	2008_DNT_T7	-19.23
77.	2012_NHA_S42	-19.23
78.	2016_VUH_T76	-19.20
79.	2009_NTTN_N3	-19.13
80.	2008_DNT_T13	-19.10
81.	2015_DON_AP1	-19.06

No.	Compound	Docking score (kJ.mol <sup>-1</sup> )
82.	2018_NHM_CF	-19.05
83.	2008_DNT_T12	-19.03
84.	2018_LTAT_C6	-18.98
85.	2018_LTAT_C4	-18.96
86.	2018_LTAT_C8	-18.93
87.	2018_LTAT_C2	-18.90
88.	2014_NGU_A2F	-18.83
89.	2013_NGU_G6	-18.73
90.	C3.5	-18.73
91.	2016_VUH_T102	-18.62
92.	2016_VUH_T101	-18.45
93.	2016_VUH_T100	-18.43
94.	C3.4	-18.41
95.	C3.1	-18.34
96.	2015_TRA_A24M	-18.30
97.	2018_LTAT_C7	-18.25
98.	2015_NGU_FME	-18.13
99.	2009_NTTN_N12	-18.11
100.	2018_LTAT_C3	-17.94
101.	2018_LTAT_C1	-17.78
102.	2009_NTTN_N7	-17.64
103.	2013_LAT_F2	-17.60
104.	2013_NGU_FH3	-17.60
105.	2009_NTTN_N8	-17.57
106.	2017_NGU_C12	-17.51
107.	TD6MC	-17.51
108.	D6	-17.40
109.	C4.4	-17.39
110.	C3.2	-17.04
111.	2007_PTPT_F14	-16.97
112.	2008_DNT_T11	-16.94
113.	2013_NGU_G7	-16.89
114.	2007_PTPT_F11	-16.24
115.	2009_HKD_Genistein	-16.23
116.	C3.6	-16.20
117.	C4.1	-16.17
118.	2018_VDD_E6	-15.65
119.	2018_VDD_D6	-15.60
120.	2016_VOD_V23	-15.38
121.	2018_VDD_EA	-13.67
122.	D5	-13.43
123.	2018_VDD_E5	-13.13
124.	2018_VDD_DA	-13.02
125.	AH6M	-12.94
126.	2018_VDD_D5	-12.90
127.	AH4M	-11.93

**Table S3.** The interaction analysis of four compound's docking poses at distal pocket AcrB

No.	Residue	Type interaction	Frequency*(%)
1	Phe 615	Surface contact	97.5
2	Phe 178	Surface contact	87.5
3	Ile 277	Surface contact	85.0
4	Gln 176	Surface contact	85.0
5	Gln 176	Hydrogen bond acceptor	72.5
6	Gly 179	Hydrogen bond donor	30.0

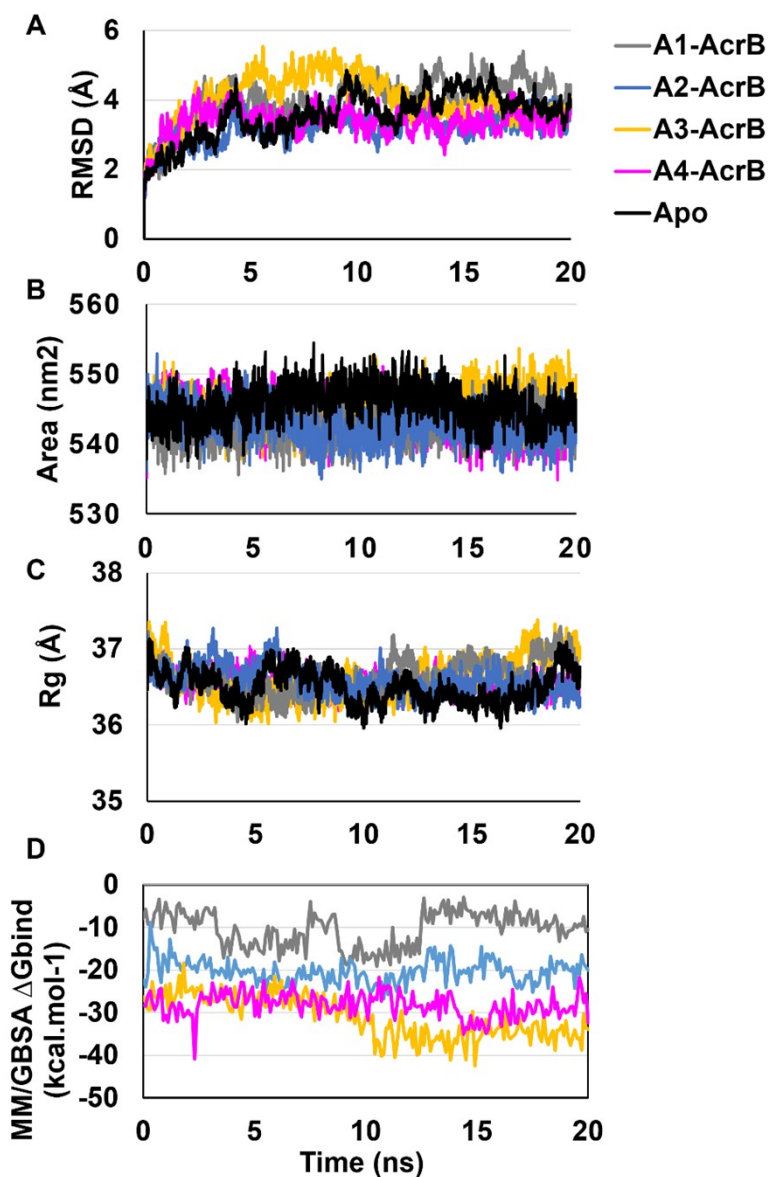
\* Only interactions with a frequency greater than or equal to 30% are presented

**Table S4.** The number and occupancy of hydrogen bonds of A4 were calculated using the data of 100 ns simulations trajectory

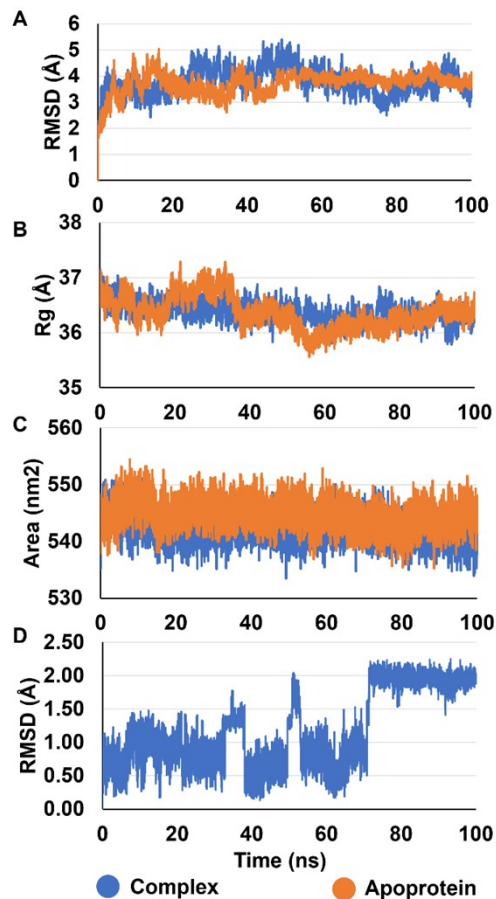
Hydrogen bonds				Arene interaction		Surface contact	
Donor		Acceptor		Residue	Occupancy	Residue	Occupancy
Residue	Occupancy	Residue	Occupancy				
Phe 628	237.77 %	Phe 628	53.01 %	Ser134	8.91 %	Phe 628	77.79 %
Ile 626	48.05 %	Val 672	43.83 %	Ile 626	6.94 %	Ser 134	63.42 %
Met 575	31.58 %	Ser 134	42.92 %	Met 573	2.87 %	Ile 626	57.76 %
Met 573	30.23 %	Gly 616	40.45 %	Phe 617	2.27 %	Met 573	48.18 %
Ser 134	26.80 %	Phe 617	24.10 %	Phe 628	1.25 %	Phe 617	11.86 %
Phe 617	30.53 %	Ser 134	16.19 %			Val 672	9.17 %
Phe 136	40.14 %					Phe 615	7.33 %
Phe 178	16.94 %					Phe 666	3.60 %
Gly 616	15.92 %					Gly 616	2.38 %
Tyr 327	15.16 %					Leu 668	2.30 %
Leu 668	14.61 %					Met 575	1.60 %
Phe 610	11.20 %					Phe 178	1.24 %

**Table S5.** The relative potential of A1-4 to reduce the MIC of LEV and OXA against *E. coli* BW25113

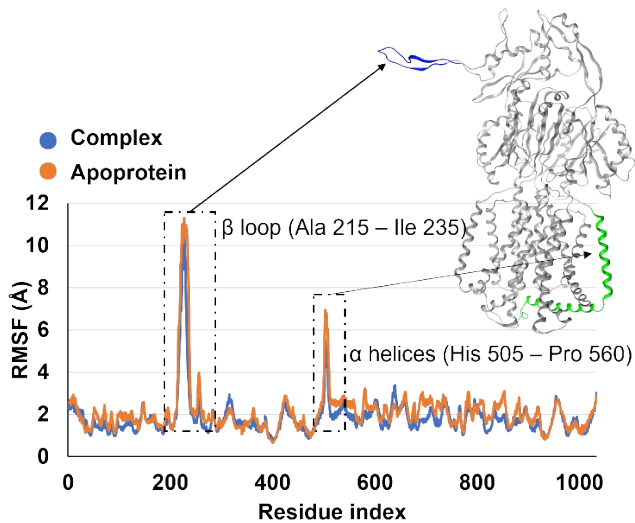
Fold reduction in MIC induced by the compound	A1			A2			A3			A4		
	200 $\mu$ M	100 $\mu$ M	50 $\mu$ M	200 $\mu$ M	100 $\mu$ M	50 $\mu$ M	200 $\mu$ M	100 $\mu$ M	50 $\mu$ M	200 $\mu$ M	100 $\mu$ M	50 $\mu$ M
OXA	2	2	1	2	2	1	2	2	1	4	2	1
LEV	1	1	1	2	2	1	2	2	1	2	2	1



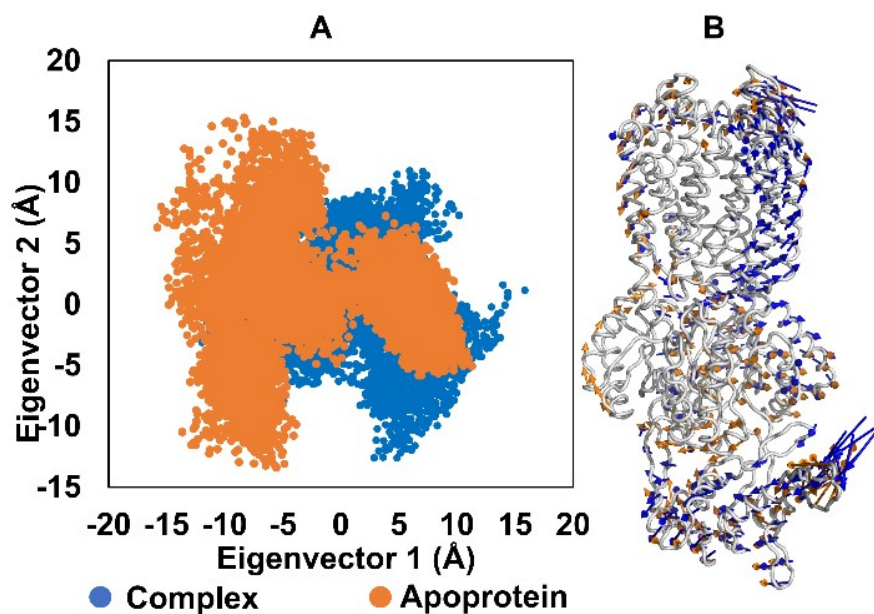
**Figure S1.** (A) RMSD value of the protein's carbon backbone; (B) Solvent accessible surface areas; (C) Radius of gyration of four complexes; (D) MM/GBSA binding free energy variation over time of four complexes are calculated using the trajectories of 20 ns MD



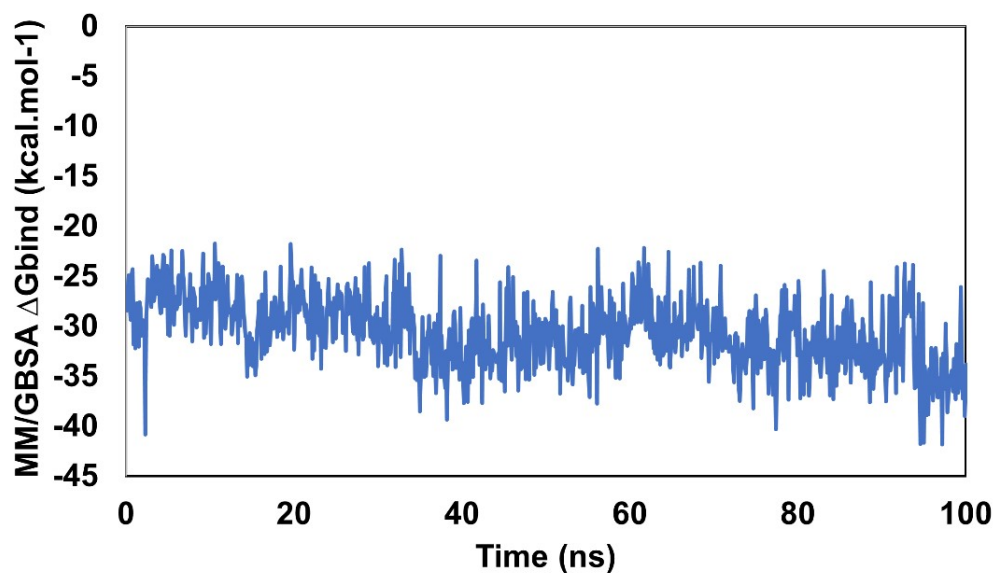
**Figure S2.** (A) Protein carbon backbone RMSD; (B) Radius of gyration; (C) Solvent accessible surface area and (D) Heavy-atom RMSD values of A4 calculated using the data of trajectories of 100 ns MD simulations



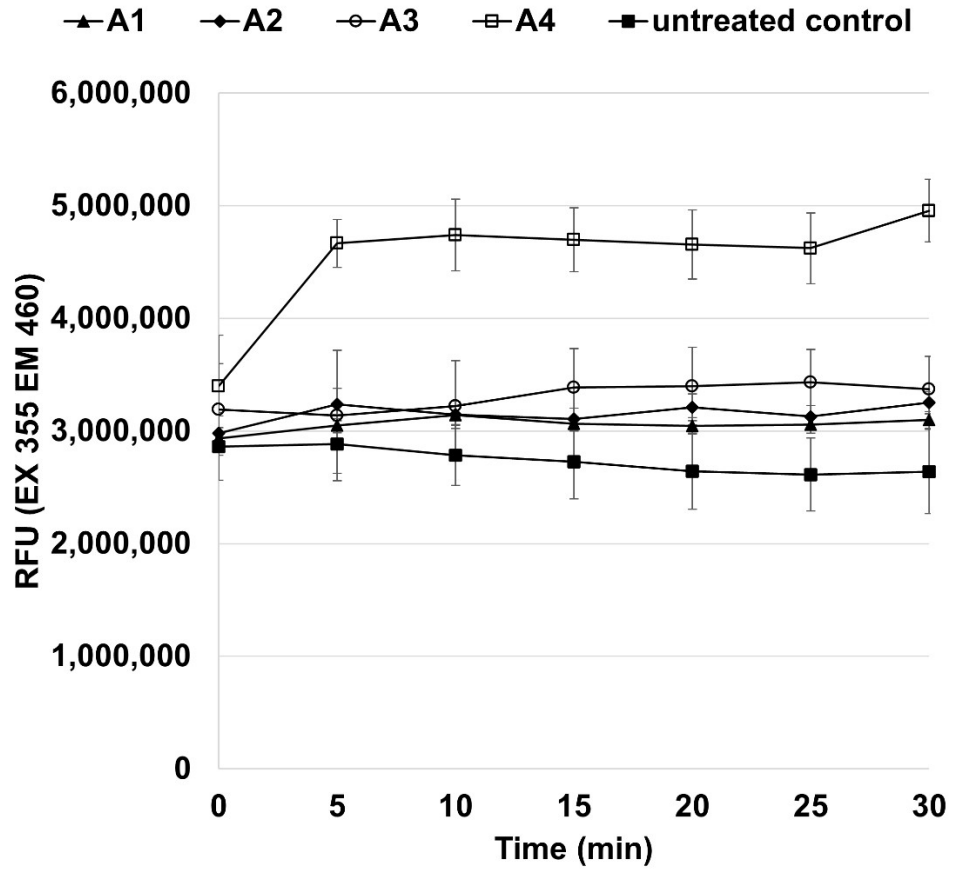
**Figure S3.** Carbon alpha RMSF values of the AcrB in apoprotein (orange) and in complex A4-AcrB (blue) were calculated using the data of 100 ns trajectories of MD simulations



**Figure S4.** Principal component analysis. (A) 2D projection of apoprotein (orange) and A4-AcrB (blue) calculated after 100 ns of MD trajectories. (B) EV1 collective motions in porcupine plot for apoprotein and A4-AcrB



**Figure S6.** MM/GBSA binding free energy variation over time of the complex is calculated using the trajectories of 100 ns MD simulations



**Figure S7.** Effects of four compounds at 100  $\mu$ M on accumulation of the fluorescent DNA-binding dye H33342, an AcrAB efflux pump substrate, in *E. coli* BW25113



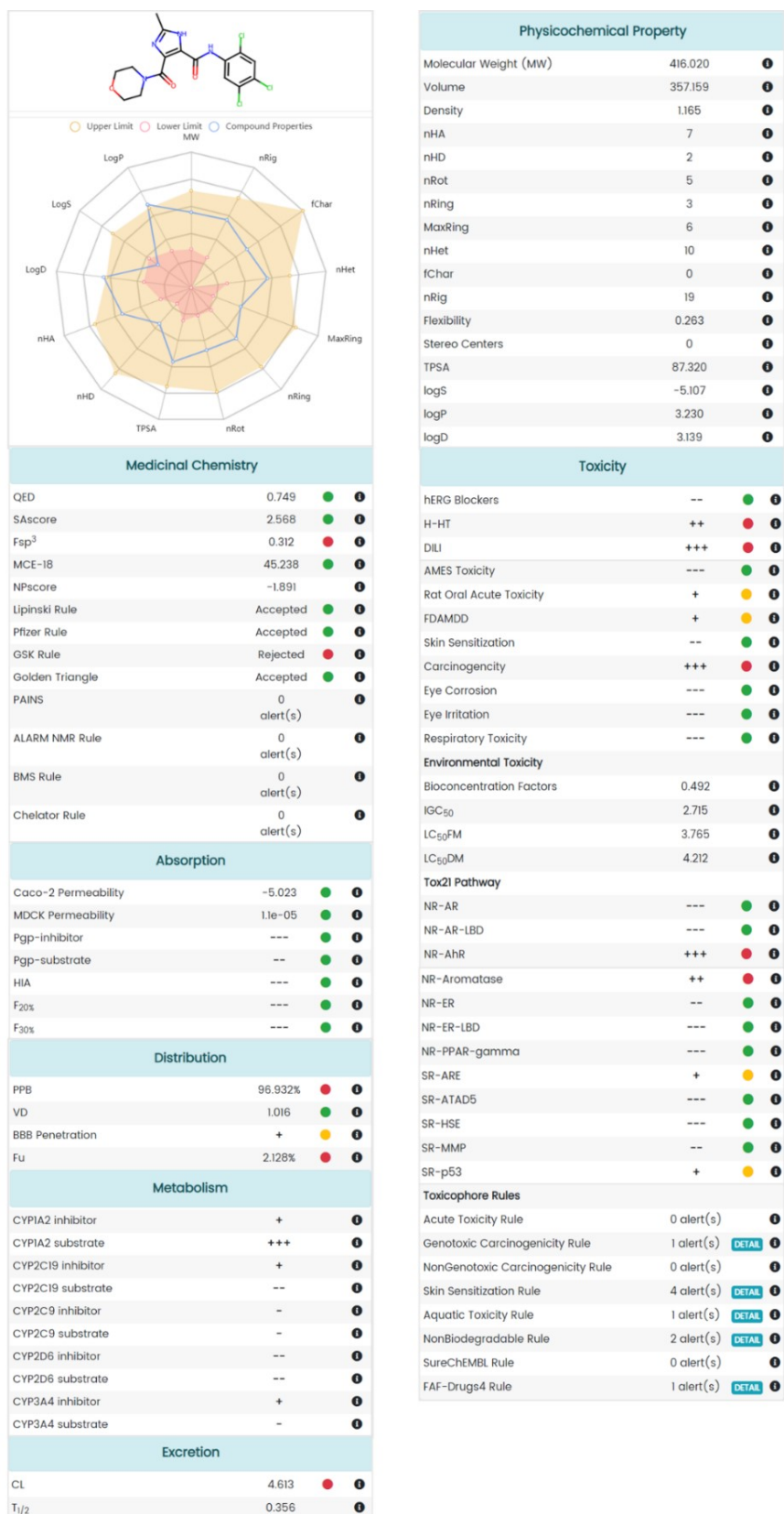


Figure S8. The A4's ADMET result generated from the ADMETlab2.0 server analyses

## Experimental

### Virtual screening

**Pharmacophore model as a rapid virtual screening tool.** For the virtual screening of molecular AcrAB-TolC inhibitors, the 2D - structure compounds were generated by MOE 2015.10.<sup>1</sup> Firstly, the compounds were energy minimized by the *Energy Minimize* tool in MOE (Forcefield: MMFF94, Gradient: 0.0001 kcal.mol<sup>-1</sup>). Secondly, the *Pharmacophore Search* tool was used to apply the pharmacophore query RHHa. The query included one aromatic ring, two hydrophobic groups and one receiving hydrogen bond group.<sup>2</sup> The compounds which satisfied the query have been subjected to molecular docking.

**Virtual screening by molecular docking model.** The compounds were prepared for the structures using Sybyl-X 2.0<sup>3</sup> prior to docking. The compounds were subjected to two iterations of energy minimization (Method: Conj Grad; Termination: Energy Change 0.0001 kcal/(mol\*A); Max Iteration: 10,000; Charges: Gasteriger-Huckel).<sup>4</sup> By using the Simulated Annealing tool, compounds were simulated molecular dynamics to overcome the energy barrier between two energy minimization phases. LeadIT<sup>5</sup> docked prepared compounds to the protein, scored, and ranked. The docking process was carried out with the following parameters: 10 poses were retained, 1000 repetitions were allowed, and 200 defragments were performed.<sup>4</sup> The data were analyzed and assessed by MOE, which validate the findings using the docking score, summarize ligand-protein interactions using *PLIF*, and identify the primary location of bonding using *Surface Map* and *Ligand Interaction*.<sup>4,6</sup>

**Molecular dynamics simulations.** MD simulations were performed using GROMACS 2020.6 software.<sup>7,8</sup> Throughout MD simulations, AcrB's chain B (1033 residues) was the only selection. The protein's topology was generated by GROMACS using the CHARMM-27 force field. The optimal docking conformation of the ligand was recorded as.mol2. The protein topology was combined with the topology of the ligand which was built using the SwissParam online tool (<https://www.swissparam.ch/>).<sup>9</sup> The box edges of simulated dodecahedron box and complex were distanced by 10 Å. Water served as the system's solvent in the TIP3P model, which added Na<sup>+</sup> or Cl<sup>-</sup> ions afterward to neutralize electricity (salt concentration was 0.15 M). With a maximum force of 10 kJ.mol<sup>-1</sup> and the steepest descent minimization, the created system's energy was minimized for 100 ps. The system was conduct to equilibrium by simulating an NVT for 100 ps to 300 K using a variable rate thermostat<sup>10</sup> and then equilibrating an NPT for 100 ps to 1 bar using a Parrinello-Rahman barostat.<sup>11</sup> The MD simulation was carried out using the Verlet method at 300 K and 1 bar of pressure. The LINCS method was used to reach the hydrogen bond limit.<sup>12</sup> Additionally, the non-bonding interactions were cut at 12 Å, and the long-range electrostatic interactions were estimated using the Mesh Ewald technique.<sup>13</sup> The MD trajectories were recorded every 0.01 ns. Using GROMACS tools, structural data from MD simulations was retrieved and examined. The root-mean-square deviation (RMSD) and root-mean-square fluctuation (RMSF) were calculated using the tools *g\_rms* and *g\_rmsf*. To investigate the dynamical stability

of simulated systems, the radius of gyration ( $R_g$ ) was calculated using *g\_gyrate* tool. Moreover, *g\_sasa* was used to assess the solvent accessible surface area (SASA) for the proteins.

**Interaction analysis.** To determine the interaction between the ligands and the residues, the occupancy of hydrogen bond formation of the ligands was investigated using VMD software.<sup>14</sup> Basic geometrical requirements specified a hydrogen bond as occurring when the angle between the hydrogen donor (D) and acceptor (A) atoms is more than 120 ° and the distance between them is less than 3.5 Å.<sup>13</sup>

**Essential dynamic.** Essential dynamic, also known as Principal component analysis (PCA) can display the apoprotein and complex's collective atomic motion, by using the *g\_covar* and *g\_anaeig* packages of GROMACS.<sup>7,15</sup> Porcupine plots were created using PyMOL to visualize the movements of the first eigenvector derived from the PCA analysis.<sup>16</sup>

**Binding free energy calculation.** Based on the single trajectory of GROMACS, calculations were carried out using the *gmx\_MMPBSA* package.<sup>17</sup> The parameters were set to 1.0 K, 298 K, and 0.15 M for the temperature, solute dielectric constant, and salt concentration, respectively.<sup>13</sup>

**Drug likeness and pharmacokinetic properties.** ADMETlab2.0 webservers were used to predict the pharmacokinetic and toxicity properties of hit compound.<sup>18</sup> The SMILES of the compound was uploaded to calculate absorption, distribution, metabolism, excretion, and toxicity properties using default parameters.

#### **Chemical synthesis**

**General chemistry information.** Room temperature is considered 27–30 °C. Reaction conditions are described in detail in the sections below. All commercially reagents and solvents from suppliers were used without further purification.

*TLC and column chromatography:* Thin-layer chromatography (TLC) was performed using TLC Silica gel 60 GF<sub>254</sub> precoated aluminium plates and the developed plates were visualized using Vilber Lourmat UV lamp. Normal phase flash column chromatography was run using silica gel 40 – 63 microns. The desired fractions from column chromatography (confirmed by TLC) were collected and concentrated under vacuum to afford the product.

*NMR:* All NMR data were collected at ambient temperature. All NMR solvents were purchased from Cambridge Isotoped. NMR spectra were processed with MestReNova software. <sup>1</sup>H-NMR spectra were obtained on Bruker 400, 500 MHz spectrometers. Proton chemical shifts were reported in ppm. Proton data were reported as chemical shifts, multiplicity (singlet (s), triplet (t), multiplet (m), ...), coupling constants [Hz] and integration. <sup>13</sup>C-NMR spectra were obtained on Bruker 100, 150 MHz spectrometer. Carbon chemical shifts were reported in ppm.

*Infrared Spectroscopy:* Infrared spectra were recorded on FTIR 8201 PC Shimadzu spectrometer, and select  $\nu_{max}$  were reported in  $\text{cm}^{-1}$ .

*Mass Spectrometry:* Mass spectrometry was conducted by Shimadzu LCMS 8040, using ESI. The HRMS was conducted by Water Xevo G2-XS Qtof.

**Synthesis of 2-methyl-imidazole-4,5-dicarboxylic acid (2).** To a 250 mL round bottom flask equipped with a magnetic stir bar, open to air, was added 2-methylbenzimidazole (6.61 g, 50 mmol), followed by concentrated sulfuric acid (50 mL). The mixture was heated to 70–80 °C and stirred until dissolved. Added last was hydrogen peroxide 30% (70 mL, 895 mmol). The reaction was heated to 110–120 °C in 2 hours. The reaction mixture was cooled to room temperature and added cold water until pH about 4. The precipitation was formed and filtered under vacuum, washed several times with water to afford the pure product.

**Synthesis of 3,8-dimethyl-5,10-dioxo-5H,10H-diimidazo[1,5- $\alpha$ :1',5'-d]pyrazine-1,6-dicarbonyl dichloride (3).** To a 100 mL round bottom flask equipped with a magnetic stir bar, was added (2) (2.17 g, 12.8 mmol), 20 mL hexane, stirred well, followed by thionyl chloride (5.6 mL, 76.8 mmol), 0.5 mL DMF. The mixture was heated to 85 °C with condenser in 16 hours. The precipitate formed in the reaction was filtered and then put back to another round bottom flask. Added 20 mL cyclohexane and heated to 85 °C in 30 mins to remove the excess thionyl chloride. The precipitate was then filtered under vacuum and washed with 10 mL cyclohexane and dried completely. This compound is sensitive to air and humidity so that it was runned some in house characterization such as melting point and IR spectroscopy.

**Synthesis of *N*<sup>1</sup>,*N*<sup>6</sup>-bis(2,4,5-trichlorophenyl)-3,8-dimethyl-5,10-dioxo-5H,10H-diimidazo[1,5- $\alpha$ :1',5'-d]pyrazine-1,6-dicarboxamide (4).** To a 50 mL round bottom flask equipped with a magnetic stir bar, was added (3) (0.68 g, 2.0 mmol), 12 mL DCM, stirred well and cooled at 0 °C. *N,N*-dimethylaniline (0.26 mL, 4.2 mmol) and aniline derivatives (4.2 mmol) were added. After 10 mins, the mixture was heated to room temperature and kept stirring in 3–16 hours. The precipitate formed in the mixture was filtered under vacuum, washed with 20 mL of DCM, 40 mL of cool water, 40 mL of acetone and dried completely. Using this method, we synthesized compounds **4a**, **4b**, **4c**, **4d**.

**Synthesis of *N*-(2,4,5-trichlorophenyl)-2-methyl-4-(morpholine-4-carbonyl)-1H-imidazole-5-carboxamide (A1-4).** To a 50 mL round bottom flask equipped with a magnetic stir bar, was added (4a-d) (1.0 mmol), 12 mL chloroform, stirred well. Morpholine (0.52 mL, 6.0 mmol) was then added. The mixture was stirred at room temperature in 16 hours. The excess of morpholine and chloroform after the reaction was removed by evaporation. The precipitate formed was washed with water to get the crude product. The crude product was purified by column chromatography over silica gel of mesh size 40 – 63 microns using an eluent mixture of chloroform – ethylacetate (1:1, v/v). Using this method, we synthesized compound **A1**, **A2**, **A3**, **A4**.

#### **Analytical Characterization Data**

**2-Methyl-imidazole-4,5-dicarboxylic acid (2).** Obtained as pale yellow solid; Yield 79,5% (6.76g); **mp** = 255-256 °C; **IR** (cm<sup>-1</sup>): 3531, 1379; **<sup>1</sup>H-NMR** (400 MHz, DMSO-*d*<sub>6</sub>)  $\delta$  (ppm): 2.49 (s, 3H); **<sup>13</sup>C-NMR** (100 MHz, DMSO-*d*<sub>6</sub>)  $\delta$  (ppm): 159.80, 146.28, 128.34, 11.68, **MS-ESI:** C<sub>6</sub>H<sub>6</sub>N<sub>2</sub>O<sub>4</sub> m/z = 170.03 (Calcd.), m/z = 168.75 [M-H]<sup>-</sup> (found).

**3,8-Dimethyl-5,10-dioxo-5H,10H-diimidazo[1,5- $\alpha$ :1',5'-d]pyrazine-1,6-dicarbonyl dichloride (3).** Obtained as pale brown solid; Yield 83.3% (1.82g); **mp** > 300 °C; **IR** (cm<sup>-1</sup>): 1757, 1344, 758.

***N*<sup>1</sup>,*N*<sup>6</sup>-diphenyl-3,8-dimethyl-5,10-dioxo-5*H*,10*H*-diimidazo[1,5-*α*:1',5'-*d*]pyrazine-1,6-dicarboxamide**

**(4a)**. Obtained as yellow solid; Yield 77.0% (0.7 g); mp = 250-251 °C, IR (cm<sup>-1</sup>): 3199, 1681, 1255.

***N*<sup>1</sup>,*N*<sup>6</sup>-bis(2-chlorophenyl)-5,10-dioxo-5*H*,10*H*-diimidazo[1,5-*α*:1',5'-*d*]pyrazine-1,6-dicarboxamide (4b)**.

Obtained as yellow solid; Yield 86.7% (0.91 g); mp = 244-246 °C, IR (cm<sup>-1</sup>): 3334, 1693, 1276.

***N*<sup>1</sup>,*N*<sup>6</sup>-bis(3,4-dichlorophenyl)-3,8-dimethyl-5,10-dioxo-5*H*,10*H*-diimidazo[1,5-*α*:1',5'-*d*]pyrazine-1,6-**

**dicarboxamide (4c)**. Obtained as yellow solid; Yield 87.0% (1.03 g); mp = 244-245 °C, IR (cm<sup>-1</sup>): 3251, 1674, 1286.

***N*<sup>1</sup>,*N*<sup>6</sup>-bis(2,4,5-trichlorophenyl)-3,8-dimethyl-5,10-dioxo-5*H*,10*H*-diimidazo[1,5-*α*:1',5'-*d*]pyrazine-1,6-**

**dicarboxamide (4d)**. Obtained as yellow solid; Yield 72.6% (0.96 g); mp = 255-256 °C, IR (cm<sup>-1</sup>): 3265, 1687, 1250.

***N*-phenyl-2-methyl-4-(morpholine-4-carbonyl)-1*H*-imidazole-5-carboxamide (A1)**. Obtained as white

solid; Yield 19.1% (0.12 g); mp = 265-267 °C, IR (cm<sup>-1</sup>): 3259, 1664, 1296; <sup>1</sup>H-NMR (600 MHz, DMSO-*d*<sub>6</sub>) δ (ppm): 13.07 (s, 0.8H), 12.82 (s, 0.2H), 12.47 (s, 0.8H), 9.81 (s, 0.2H), 7.79 (s, 0.4H), 7.63 (d, 1.6H, *J* = 6.5 Hz), 7.37 (t, 1.6H, *J* = 6.5 Hz), 7.30 (s, 0.4H), 7.11 (t, 0.8H, *J* = 6.0 Hz), 7.06 (s, 0.2H), 4.17-3.40 (m, 8H), 2.34 (s, 3H); <sup>13</sup>C-NMR (150 MHz, DMSO-*d*<sub>6</sub>) δ (ppm): 164.14, 156.50, 145.00, 138.47, 133.10, 129.72, 129.04, 123.68, 119.17, 66.38, 66.08, 47.95, 43.10, 13.48; HRMS-ESI: C<sub>16</sub>H<sub>18</sub>N<sub>4</sub>O<sub>3</sub> m/z = 314.13789 (Calcd.), m/z = 315.14822 [M+H]<sup>+</sup> (found).

***N*-(2-chlorophenyl)-2-methyl-4-(morpholine-4-carbonyl)-1*H*-imidazole-5-carboxamide (A2)**. Obtained as

white solid; Yield 24.4% (0.17 g); mp = 223-225 °C, IR (cm<sup>-1</sup>): 3242, 1653, 1285; <sup>1</sup>H-NMR (500 MHz, CDCl<sub>3</sub>) δ (ppm): 12.26 (s, 1H), 11.50 (s, 1H), 8.12 (dd, 1H, <sup>3</sup>*J* = 8.0 Hz, <sup>4</sup>*J* = 1.5 Hz), 7.44 (dd, 1H, <sup>3</sup>*J* = 8.0 Hz, <sup>4</sup>*J* = 1.5 Hz), 7.27 (td, 1H, <sup>3</sup>*J* = 7.5 Hz, <sup>4</sup>*J* = 1.5 Hz), 7.12 (td, <sup>3</sup>*J* = 7.5 Hz, <sup>4</sup>*J* = 1.5 Hz), 4.26 (t, 2H, *J* = 5.0 Hz), 3.84-3.78 (m, 4H), 3.75 (t, 2H, *J* = 5.0 Hz), 2.36 (s, 3H); <sup>13</sup>C-NMR (125 MHz, DMSO-*d*<sub>6</sub>) δ (ppm): 163.69, 160.32, 159.50, 157.10, 145.52, 144.96, 134.91, 134.60, 133.95, 130.83, 129.58, 129.27, 128.78, 127.87, 127.49, 127.03, 125.63, 124.81, 124.31, 124.04, 122.82, 122.43, 66.48, 66.16, 66.07, 65.82, 47.80, 46.90, 42.96, 41.93, 13.50; HRMS-ESI: C<sub>16</sub>H<sub>17</sub>ClN<sub>4</sub>O<sub>3</sub> m/z = 348.09892 (Calcd.), m/z = 371.08995 [M+Na]<sup>+</sup> (found) for <sup>35</sup>Cl isotope and m/z = 373.08748 [M+Na]<sup>+</sup> (found) for <sup>37</sup>Cl isotope, the ratio at 3:1.

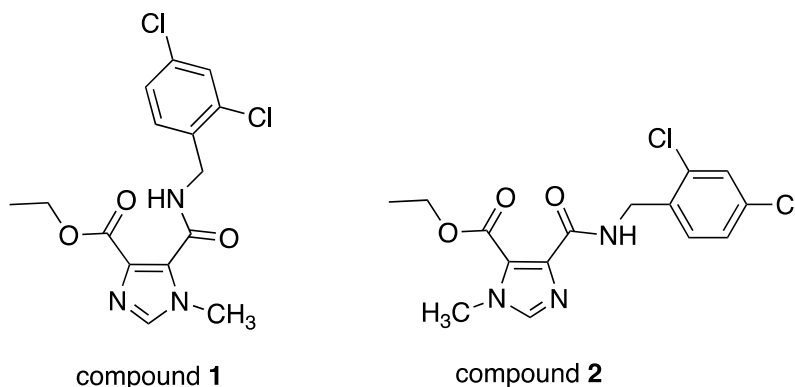
***N*-(3,4-dichlorophenyl)-2-methyl-4-(morpholine-4-carbonyl)-1*H*-imidazole-5-carboxamide (A3)**. Obtained

as white solid; Yield 31.3% (0.24 g); mp = 261-263 °C, IR (cm<sup>-1</sup>): 3257, 1678, 1269; <sup>1</sup>H-NMR (600 MHz, DMSO-*d*<sub>6</sub>) δ (ppm): 13.09 (s, 1H), 12.85 (s, 0.7H), 10.26 (s, 0.3H), 8.07 (s, 1H), 7.61-7.50 (m, 2H), 4.18-3.63 (m, 8H), 2.35 (s, 3H); <sup>13</sup>C-NMR 164.03, 160.61, 160.54, 156.83, 145.50, 144.64, 139.05, 138.47, 133.65, 131.33, 131.27, 131.02, 130.72, 130.34, 129.30, 127.42, 125.19, 124.64, 121.22, 120.39, 120.05, 119.39, 66.40, 66.10, 65.96, 65.93, 48.05, 42.26, 13.54, 13.45; HRMS-ESI: C<sub>16</sub>H<sub>16</sub>Cl<sub>2</sub>N<sub>4</sub>O<sub>3</sub> m/z = 382.05995 (Calcd.), m/z = 383.06926 [M+H]<sup>+</sup> (found) for two <sup>35</sup>Cl isotopes, m/z = 385.06653 [M+H]<sup>+</sup> (found) for one <sup>35</sup>Cl isotope and one <sup>37</sup>Cl isotope, and m/z = 387.06412 [M+H]<sup>+</sup> (found) for two <sup>37</sup>Cl isotopes.

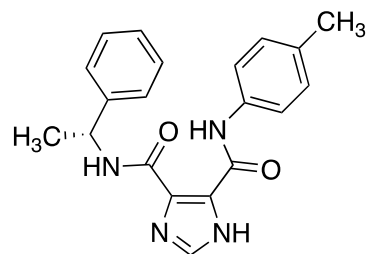
***N*-(2,4,5-trichlorophenyl)-2-methyl-4-(morpholine-4-carbonyl)-1*H*-imidazole-5-carboxamide (A4).**

Obtained as white solid; Yield 38.3% (0.32g); mp = 261-263 °C, IR (cm<sup>-1</sup>): 3342, 1645, 1288; <sup>1</sup>H-NMR (500 MHz, CDCl<sub>3</sub>) δ (ppm): 12.61 (s, 1H), 11.12 (s, 1H), 8.50 (s, 1H), 7.55 (s, 1H), 4.33 (t, 2H, *J* = 5.0 Hz), 3.84 (m, 4H), 3.79 (t, 2H, *J* = 5.0 Hz), 2.48 (s, 3H); <sup>13</sup>C-NMR (150 MHz, DMSO-*d*<sub>6</sub>) δ (ppm): 163.42, 157.26, 145.87, 135.24, 134.32, 130.54, 129.83, 128.45, 126.24, 123.67, 123.89, 66.40, 66.10, 47.75, 42.99, 13.51, HRMS-ESI: C<sub>16</sub>H<sub>15</sub>Cl<sub>3</sub>N<sub>4</sub>O<sub>3</sub> m/z = 416.02097 (Calcd.), m/z = 417.02747 [M+H]<sup>+</sup> (found).

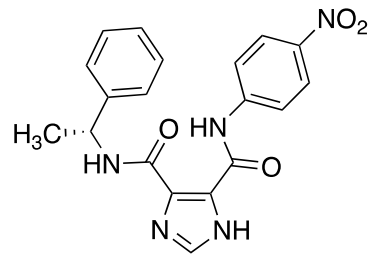
The compounds **A1-A4** were determined by <sup>1</sup>H-NMR spectra in DMSO-*d*<sub>6</sub>, CDCl<sub>3</sub> solvents. In the <sup>1</sup>H-NMR spectra measured in DMSO-*d*<sub>6</sub> solvent, the highest chemical shift peak was the H atom of NH in the imidazole ring while in the CDCl<sub>3</sub>, the highest one was the H atom in the amide bond (*Crystal growth & design*. 2006;6(9):2047-2052. doi:10.1021/cg060057i; *Organic letters*. 2005;7(1):135-138. doi:10.1021/ol047812a). According to the study of Yasuda N. et al. about the formation of intramolecular hydrogen bonds of imidazole-4-carboxylic acid ester-5-carboxamide derivatives, compound **1** and **2** were isomers but only compound **1** was shown to have an intramolecular hydrogen bond while compound **2** was not (*Journal of heterocyclic chemistry*. 1987;24(2):303-307. doi:10.1002/jhet.5570240202P).



This interaction was shown by the chemical shift of H atom in the NH amide bond. If this H atom (of NH amide) participated in intramolecular hydrogen bonding, the chemical shift of the H atom would move to the lower field region. On the <sup>1</sup>H-NMR spectrum of compound **1** in CDCl<sub>3</sub> solvent, the H peak of NH amide had the higher chemical shift of 10.67 ppm compared with a similar H peak in compound **2** shown in the <sup>1</sup>H-NMR spectrum in the same solvent having the chemical shift of 8.09 ppm. This difference was used by Yasuda N. to conclude that compound **1** formed intramolecular hydrogen bonds but compound **2** did not (*Journal of heterocyclic chemistry*. 1987;24(2):303-307. doi:10.1002/jhet.5570240202P). The intramolecular hydrogen bond in compound **1** was formed by H of the NH amide with the O atom in the C=O of the ester group. In addition, according to the study by Baures et al. on the intramolecular hydrogen bonding of imidazole-4,5-dicarboxamide derivatives, the H peak of the NH amide with aniline derivatives in CDCl<sub>3</sub> when participating in intramolecular hydrogen bonding had the chemical shift more than 13 ppm while the H peak when not in intramolecular hydrogen bonding had the chemical shift of 9.36–9.79 ppm (compound **3** and **4**) (*Organic letters*. 2005;7(1):135-138. doi:10.1021/ol047812a).



compound 3



compound 4

It was found that in the  $^1\text{H-NMR}$  spectra in  $\text{CDCl}_3$  of compound **A2** and **A4**, the chemical shift of NH amide moved to the lower field than the NH amide in compound **1** and the NH amide of aniline derivatives in compound **3** and **4** when not participating in intramolecular hydrogen bonding. It can be concluded that compound **A2** and **A4** in  $\text{CDCl}_3$  the NH of the amide group was in a state of forming intramolecular hydrogen bonding. In the  $^1\text{H-NMR}$  spectra in  $\text{DMSO-}d_6$  solvent of compound **A1** and **A3**, the NH amide peak was splitted into 2 peaks and the one at lower field indicated that the H atom was in the state of intramolecular hydrogen bonding. The intramolecular hydrogen bonding in these compounds may form from the NH amide of aniline derivatives with O atom in amide bond with morpholine, which was similar to the reported imidazole-4,5-dicarboxamide derivatives (*Journal of medicinal chemistry*. 2005;48(19):5955-5965.doi:10.1021/jm050160r). For the compound **A3**, the  $^1\text{H-NMR}$  spectrum in  $\text{DMSO-}d_6$  recorded the separation of peak H atom of NH amide at the ratio 7:3 in which the higher proportion when the H atom of the NH amide was in the state of intramolecular hydrogen bonding indicated by the lower field peak. Similarly, the compound **A1**, the  $^1\text{H-NMR}$  spectrum in  $\text{DMSO-}d_6$  recorded the separation of peak H atom of NH amide at the ratio 8:2.

#### Structural elucidation of **A1**:

Compound **A1** was obtained as white solid and its molecular formula was established as  $\text{C}_{16}\text{H}_{18}\text{N}_4\text{O}_3$  through the  $m/z$  315.1482  $[\text{M}+\text{H}]^+$  (found), 315.1457 (Calcd.) in the HRES-EMS spectrum. The combination of  $^{13}\text{C-NMR}$  and HSQC spectra of **A1** showed the presence of 16 main carbon signals. Based on the HSQC spectrum, all of proton signals in **A1** were determined including five aromatic protons (H17-H21); four  $-\text{CH}_2$  groups (H9-H10, H12-H13); and one methyl group (H6) together with two proton signals of  $-\text{NH}$  group (H1 and H15). In the HMBC analysis, the correlation of proton and carbon were showed to confirm the structure of **A1** (Figure S5).

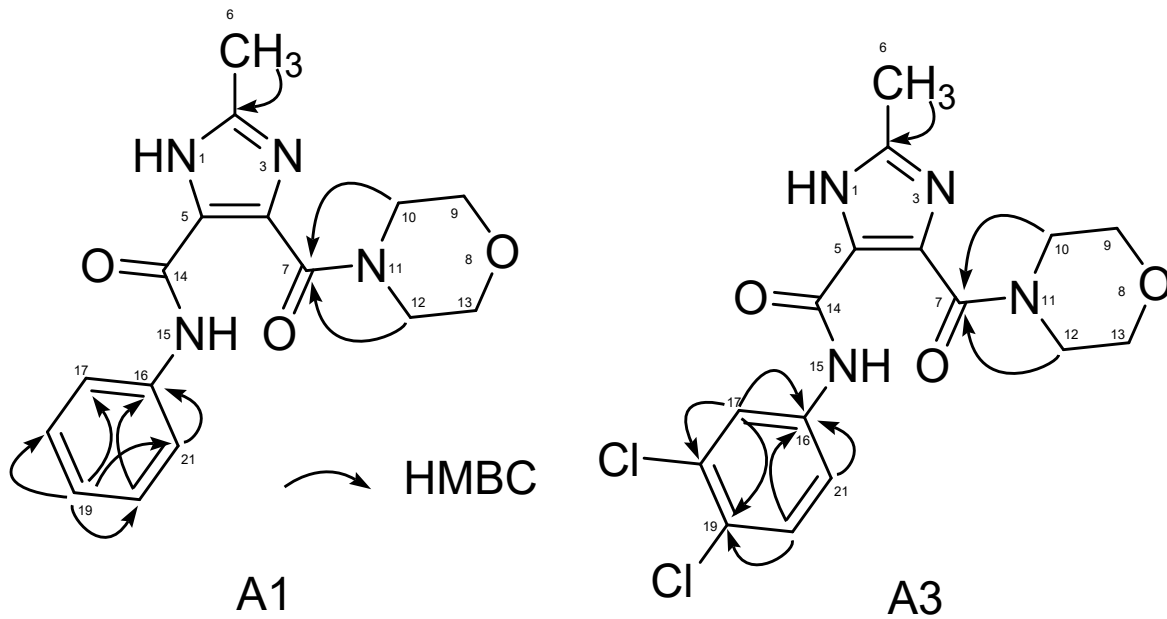
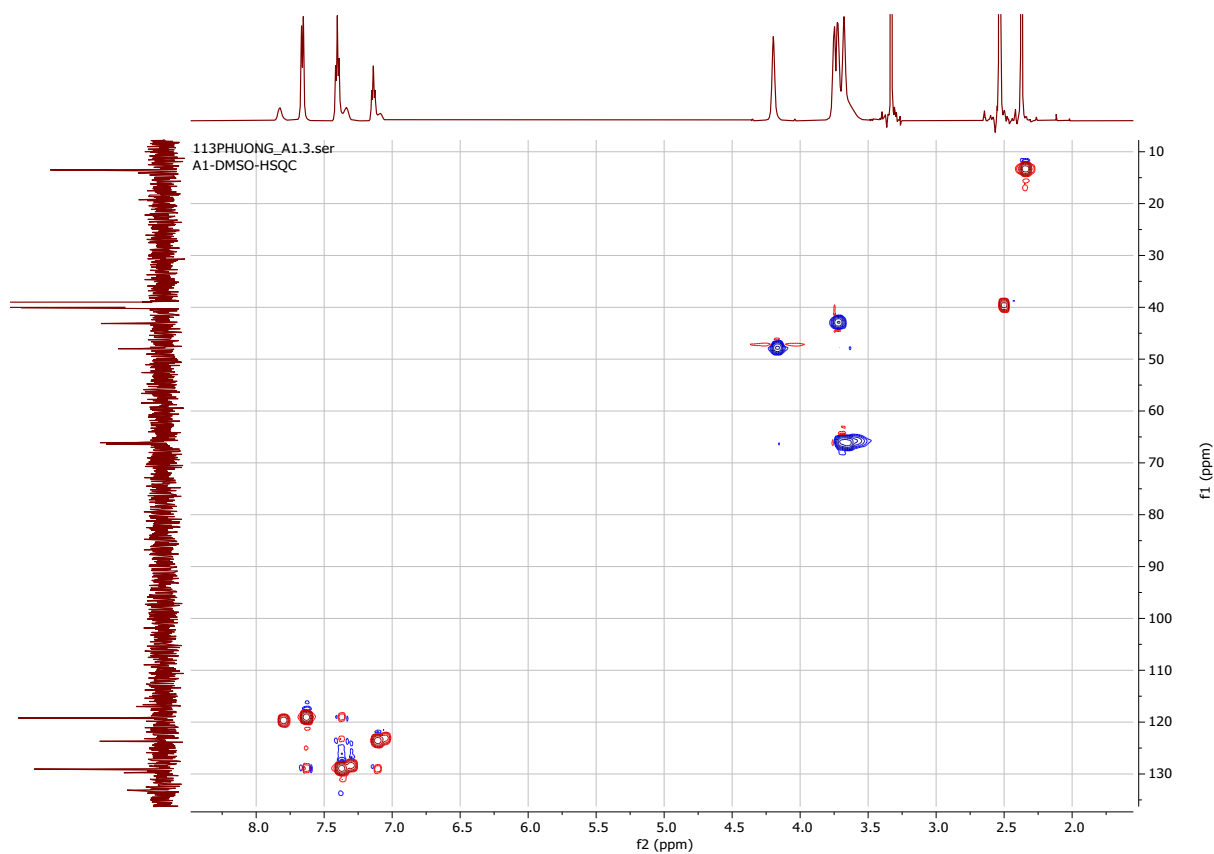
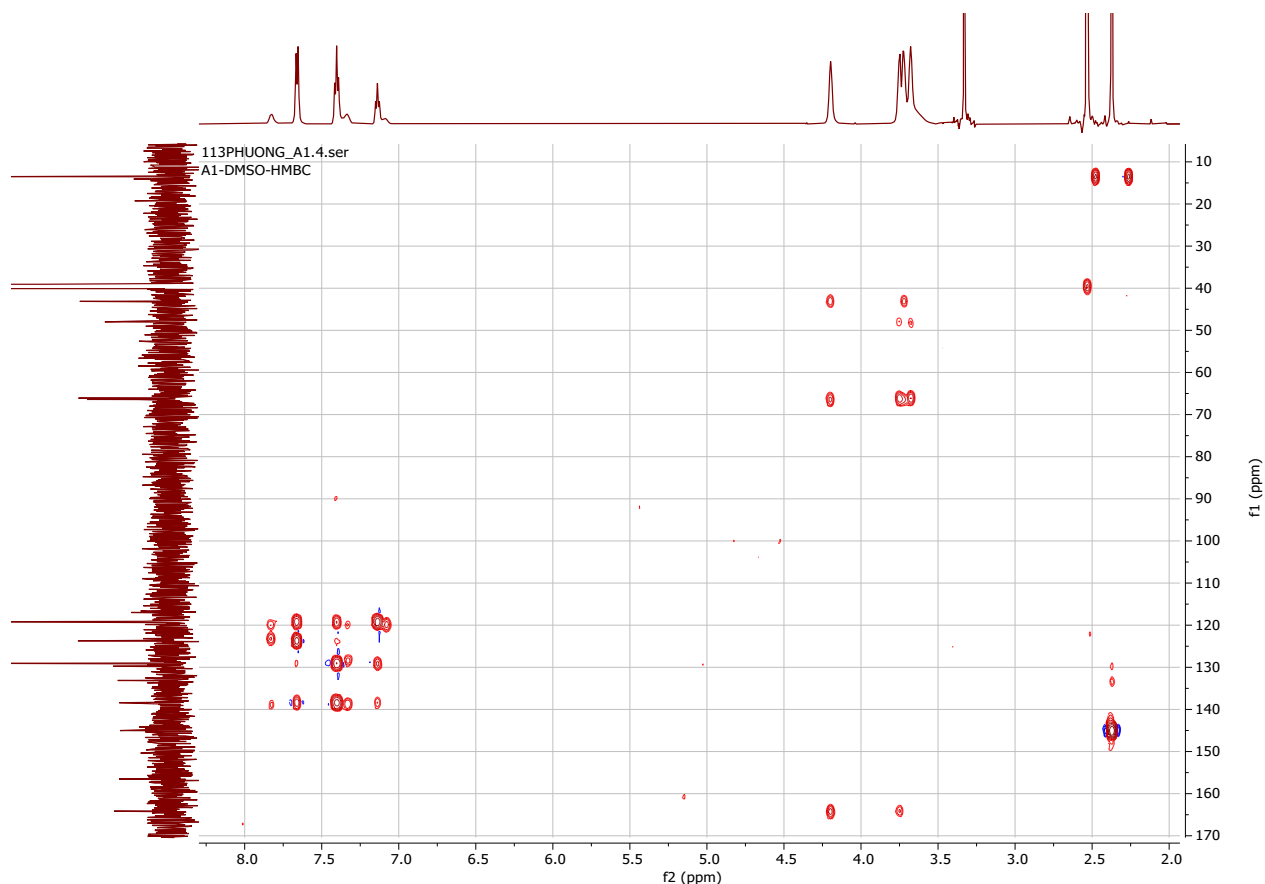


Figure S5. HMBC correlations observed for compounds **A1** and **A3**



HSQC spectrum of **A1** in DMSO-*d*<sub>6</sub>





HMBC spectrum of **A1** in DMSO-*d*<sub>6</sub>

Calculation of forming energy of intrahydrogen bonding and non-intrahydrogen bonding isomers of compounds **A1**, **A3** in DMSO<sup>19</sup>

The MOPAC software was used with the input .mop files (The structures of compounds were prepared by Chemdraw, transferred to 3D structure by Chem3D, optimized the energy by Chem3D using MM2 method. The files were saved as .mop files). The calculation was carried by MOPAC with some properties: gnorm = 0.01, eps = 46.7, precise pm7 1scf. The results were reported in the table belowed.

Calculation	<i>intrahydrogen bonding A1</i>	<i>non-intrahydrogen bonding A1</i>	<i>intrahydrogen bonding A3</i>	<i>non-intrahydrogen bonding A3</i>
Heat of formation (kcal/mol)	13.71441	23.93299	-4.90964	5.04046
Van Der Waals area (square angstrom)	317.86	318.28	354.75	354.99
Dielectric energy (ev)	-1.00950	-1.73167	-1.01825	-1.81587
Ionization potential (ev)	9.138265	9.150611	9.288913	9.200537

Homo lumo energies (ev)	-9.318; -1.001	-9.151; -1.038	-9.289; -1.139	-9.201; -1.163
Cosmo area (square angstrom)	317.86	318.28	354.75	354.99
Cosmo volume (cubic angstrom)	350.96	351.39	396.07	396.92

**Calculation of the percentage of intrahydrogen bonding and non-intrahydrogen bonding isomers of compounds A1 and A3 in DMSO at room temperature.**

The heat of formation  $\Delta H^\circ$  of intrahydrogen bonding and non-intrahydrogen bonding isomers predicted by MOPAC software were used to calculate  $\Delta H^\circ_{\text{rxn}}$  of this equilibrium:

Intrahydrogen bonding isomer  $\leftrightarrow$  non-intrahydrogen bonding isomer

**Using the van't Hoff equation** <sup>20</sup>

$$\ln \frac{K_1}{K_0} = - \frac{\Delta H_{\text{rxn}}}{R} \left( \frac{1}{T_1} - \frac{1}{T_0} \right)$$

to calculate the constants of the equilibrium at 298K, the experimental constants at 303.1K (temperature at which the <sup>1</sup>H-NMR was taken).

**For compound A1:  $K_{303.1\text{K}} = 1/4$ ,  $\Delta H^\circ_{\text{rxn}} = 42754.54 \text{ J/mol} \Rightarrow K_{298.0\text{K}} = 0.19 \Rightarrow$  ratio of intrahydrogen bonding isomer of A1/ non-intrahydrogen bonding isomer of A1 = 0.84/0.16.**

For compound A3:  $K_{303.1\text{K}} = 3/7$ ,  $\Delta H^\circ_{\text{rxn}} = 41631.2 \text{ J/mol} \Rightarrow K_{298.0\text{K}} = 0.32 \Rightarrow$  ratio of intrahydrogen bonding isomer of A3/ non-intrahydrogen bonding isomer of A3 = 0.76/ 0.24.

**Biological assay**

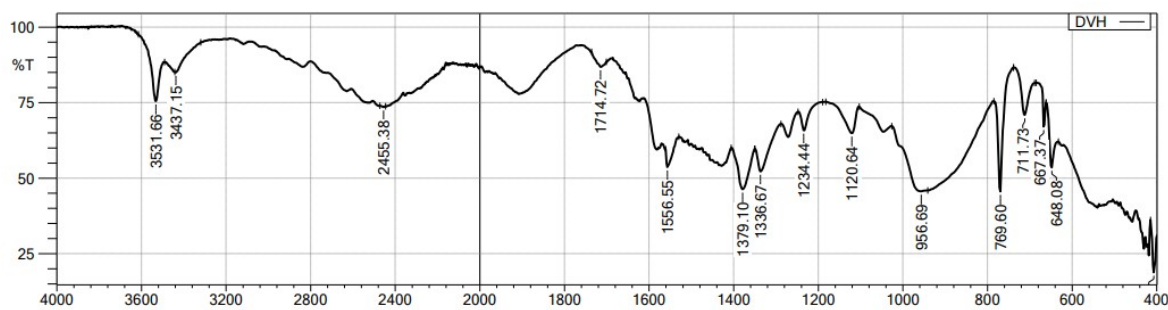
**Strains and reagents.** The following strains were obtained from the Keio collection<sup>21</sup>: *E. coli* BW25113 (WT), JW0451 ( $\Delta\text{acrB}::\text{kan}$ ), and JW0453 ( $\Delta\text{acrR}::\text{kan}$ ). The following reagents were purchased from Sigma-Aldrich (St. Louis, MO): bisBenzimide Hoechst 33342 trihydrochloride (H33342), Levofloxacin (LEV) and Oxacillin (OXA). NMP was purchased from Alfa Aesar by Thermo Fisher Scientific (USA). Luria-Bertani (LB) broth and phosphate-buffered saline (PBS) were purchased from Himedia (India).

**Antibacterial activity assays.** In general, the CLSI protocol M7-A7's description of the broth microdilution method was used to determine the Minimum Inhibitory Concentration (MIC) of antibacterial agents. Stock cultures of bacteria were sub-cultured onto Mueller Hinton Agar (MHA) plates and incubated at 37 °C for an entire night. On the second day, three to five distinct bacterial colonies with comparable morphology were inoculated into sterile Mueller Hinton broth (MHB), and bacterial suspensions were adjusted to 0.5 McFarland (about  $1\text{-}2 \times 10^8$  CFU/ml). In a 96-well round-bottom microtiter plate, the assay consisted of one column of broth sterility control, one column of growth control, one vertical row of antibiotic control, and finally one column of each test sample. Serial 2-fold dilutions of test compounds were made in dimethyl

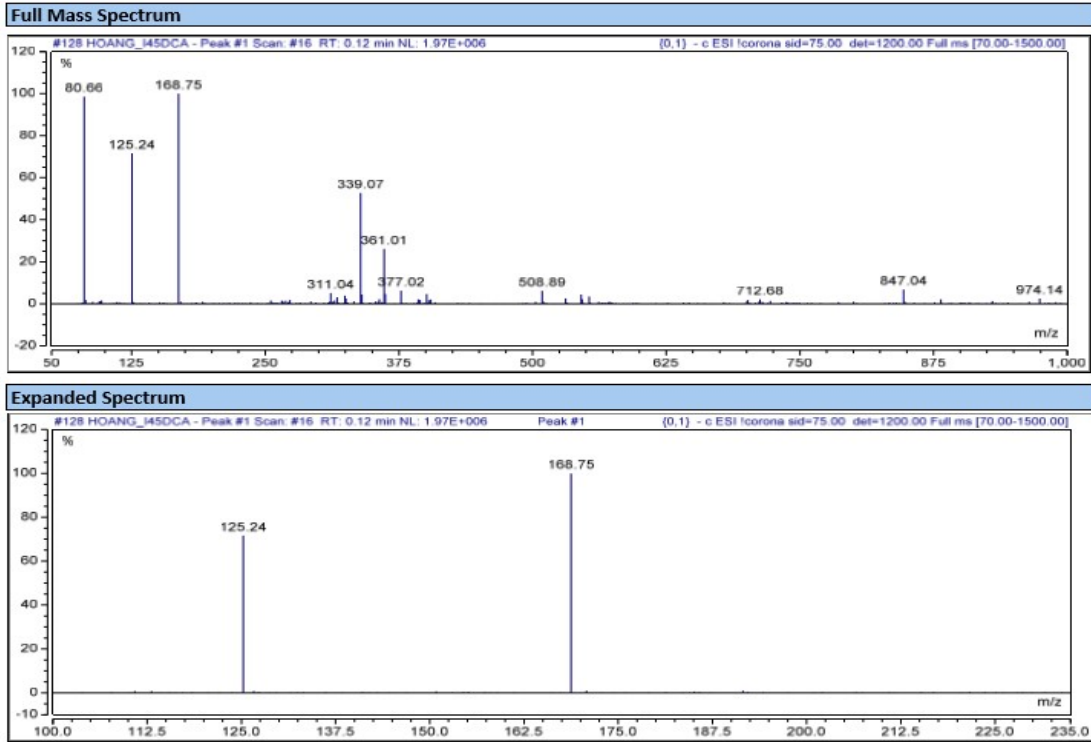
sulfoxide (DMSO) at concentrations 40-fold higher than the final concentration; the diluted compounds were added to the assay plates, and 100  $\mu$ l of the bacterial culture was added to each well. The final concentration of DMSO in each assay was 2.5%. A final concentration of an EPI ranging from 50 to 200  $\mu$ M was used in the MIC tests as specified. The geometric mean was computed after MIC assays were carried out in triplicate. To illustrate the inhibitory effects of extracts or compounds, the resazurin-based turbidometric test was used.<sup>22,23</sup> After overnight incubation at 37 °C, resazurin (5  $\mu$ l; 6.75 mg.ml<sup>-1</sup>) was applied to all wells and incubated at 37 °C for 4 hours.<sup>22</sup> Color variations were observed and recorded. The MIC was defined as the lowest concentration at which the color did not change. Using the same modifications as for the MIC tests mentioned above, checkerboard MIC assays with an EPI and an antibacterial agent were carried out essentially as previously described.<sup>22,23</sup>

**H33342 accumulation assay.** Essentially as described previously, the H33342 accumulation assay was utilized to assess how EPIs affected the activity of the AcrAB-TolC efflux pump in bacteria.<sup>24,25</sup> Bacteria were cultured overnight in LB with aeration at 37 °C before being used to inoculate fresh cultures (1:100 dilution), which were then grown in LB with aeration until an optical density at 600 nm (OD<sub>600</sub>) of 0.8 to 1.0 was attained. A volume of phosphate-buffered saline (PBS) containing 22 mM glucose (PBS+G) comparable to the original volume of the culture was used to wash the cell pellet after bacterial cells were retrieved by centrifugation. The cell pellets were then resuspended in PBS+G after centrifugation, and the OD<sub>600</sub> of each suspension was adjusted to 0.35. 175  $\mu$ l aliquots were added to the wells of a 96-well assay plate (flat-bottom black plate, no. 3515; Costar, Corning, NY). For each of the conditions examined, three assay wells (one column of wells) were added with 5  $\mu$ l of test chemicals dissolved in DMSO. In all experiments, the final DMSO concentration was 2.5 %. 20  $\mu$ l of a solution of 25  $\mu$ M H33342 in PBS+G was added to each test well after the assay plates had been incubated at 37 °C for 15 min, yielding a final dye concentration of 2.5  $\mu$ M. Using a Victor Nivo™ Multimode Plate Reader, the fluorescence of each well was measured at room temperature every five minutes for thirty minutes using excitation and emission filters of 355 nm and 460 nm, respectively (PerkinElmer, Waltham, MA). Microsoft Excel was used to obtain the average values and standard deviations for the three replicates for each condition.

### The NMR Assignments, Infrared Spectroscopy and Mass Spectrum of synthetic compounds

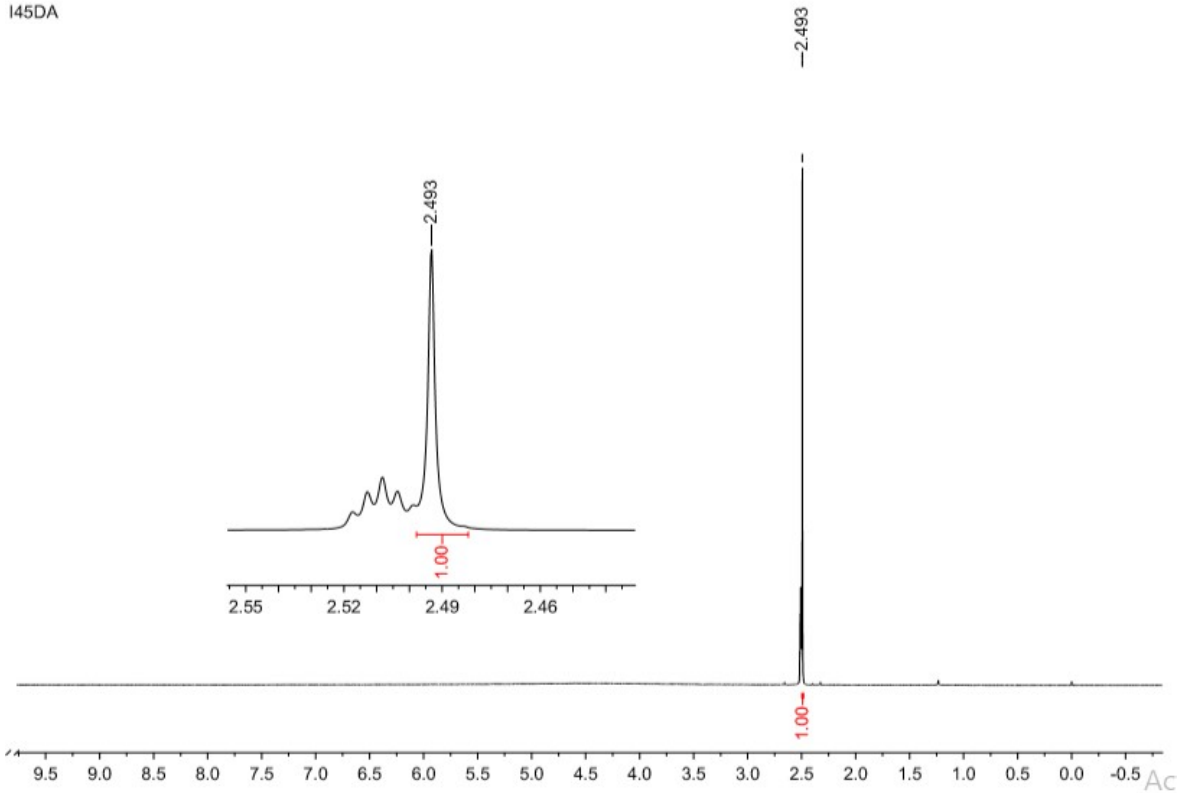


## IR spectrum of compound 2

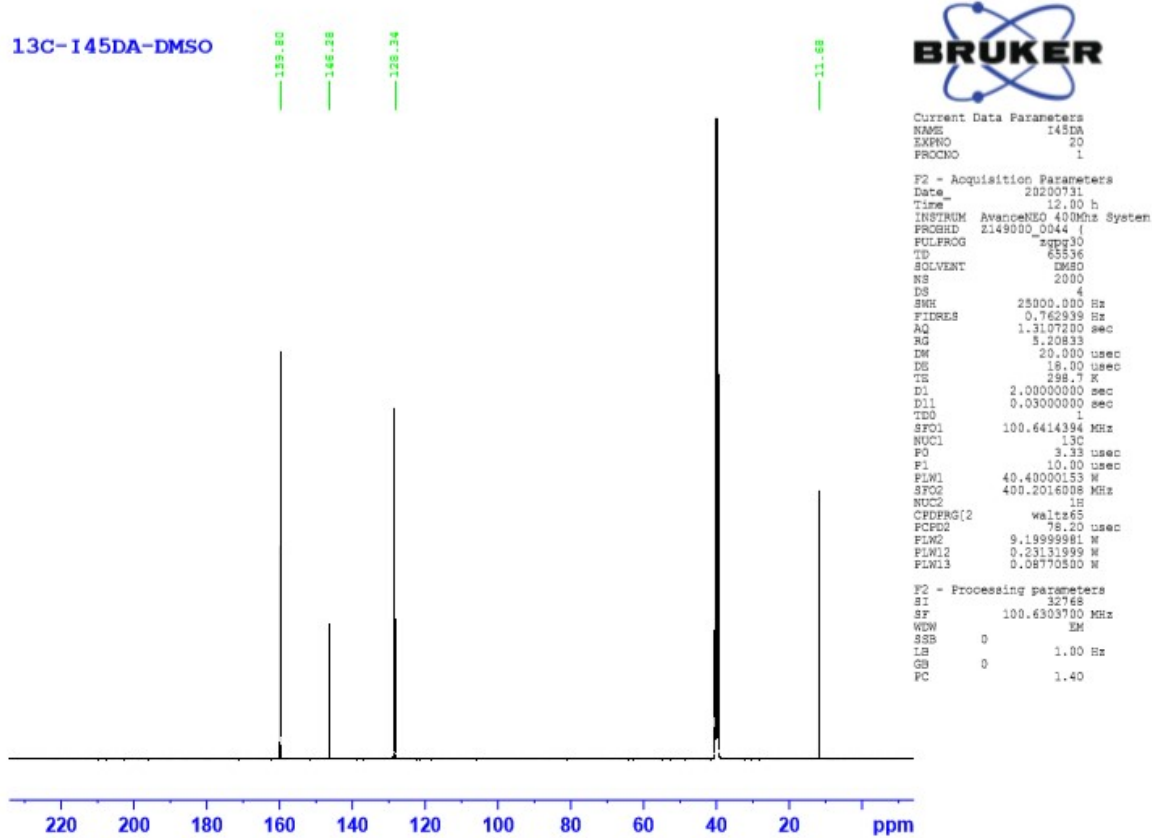


## Mass spectrum of compound 2

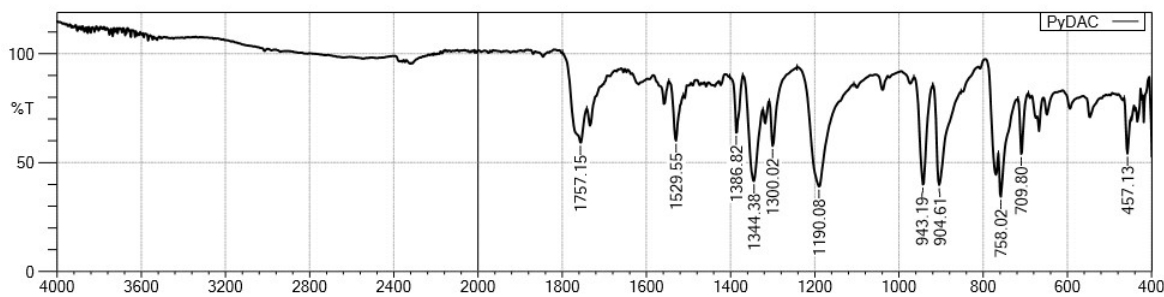
I45DA



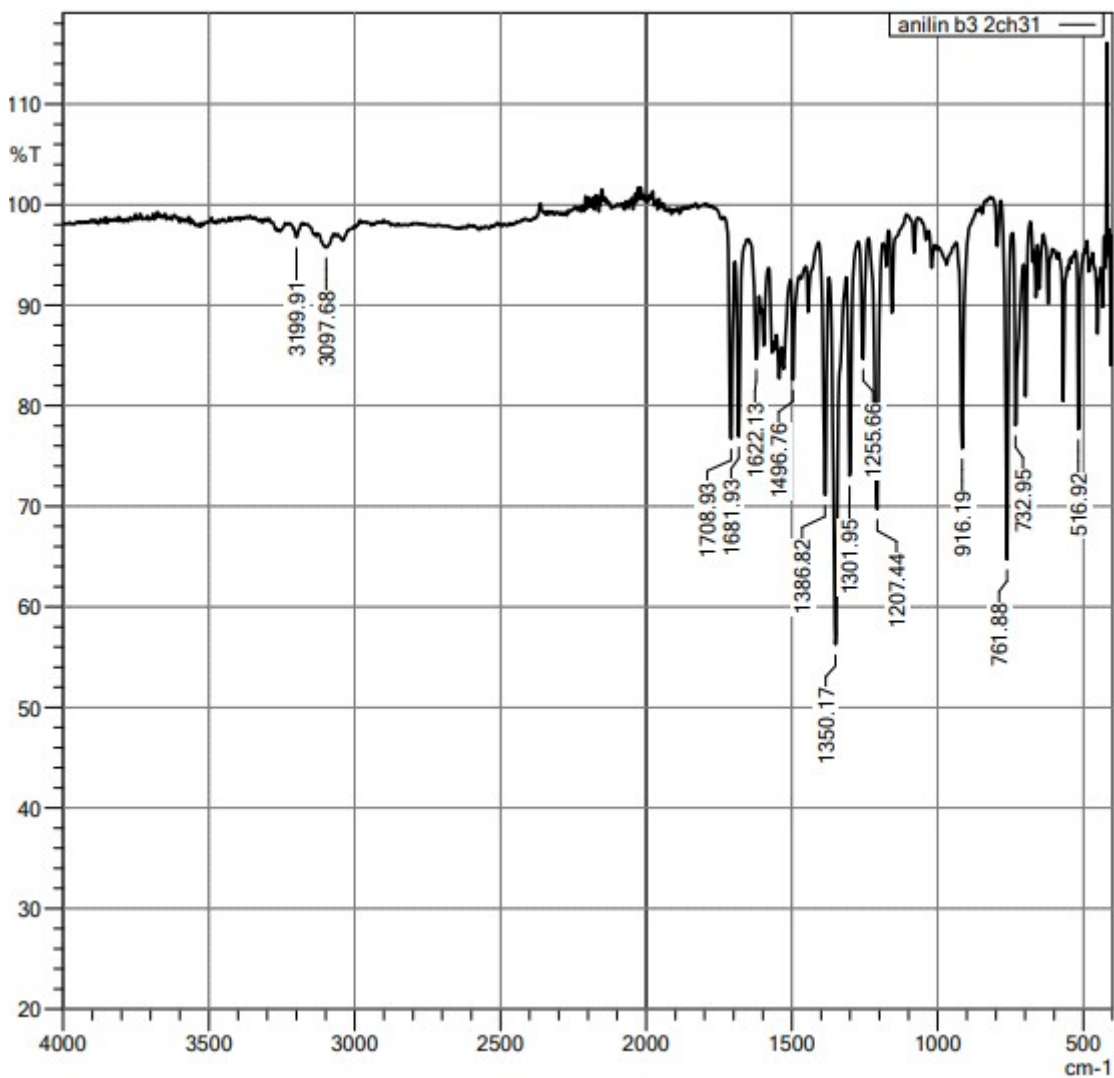
<sup>1</sup>H-NMR spectrum of compound 2



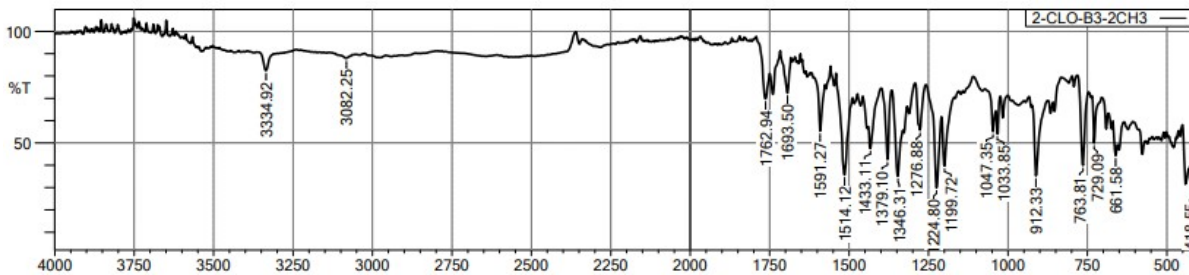
<sup>13</sup>C-NMR spectrum of compound 2



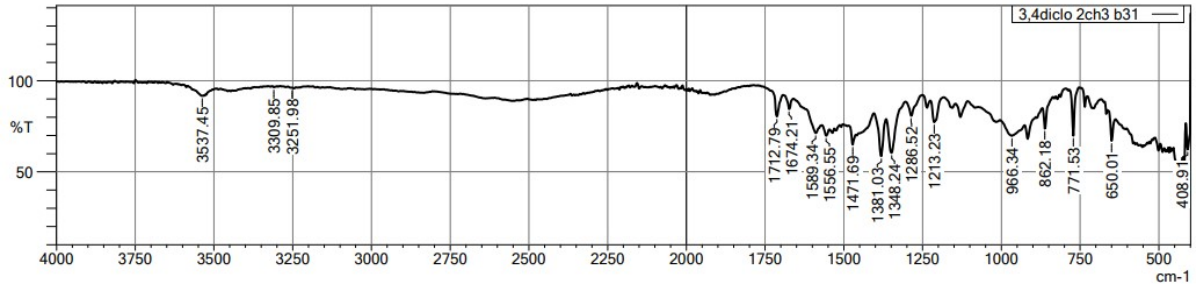
IR spectrum of compound 3



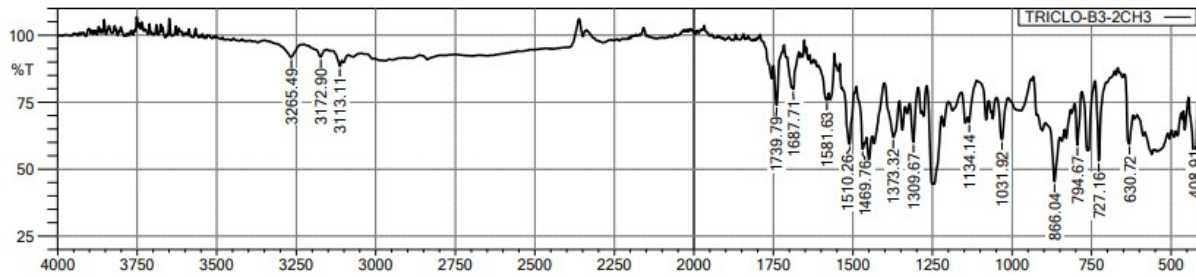
IR spectrum of compound 4a



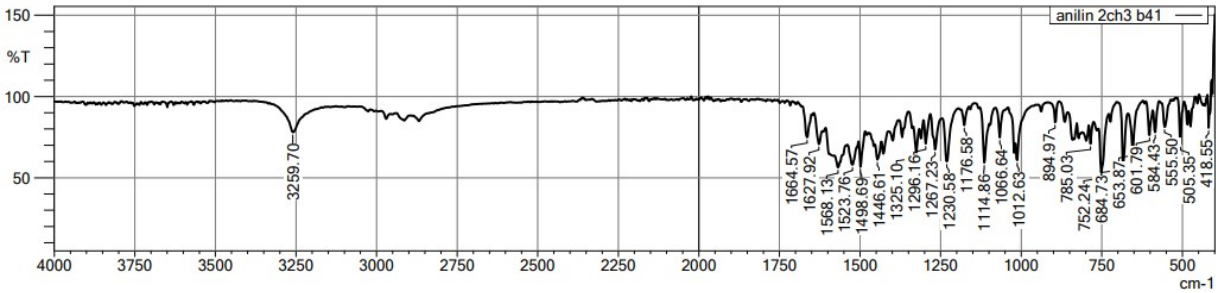
IR spectrum of compound 4b



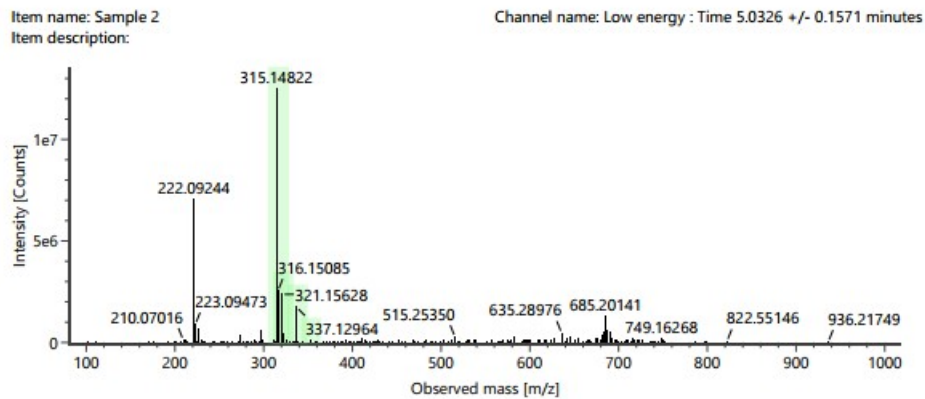
IR spectrum of compound 4c



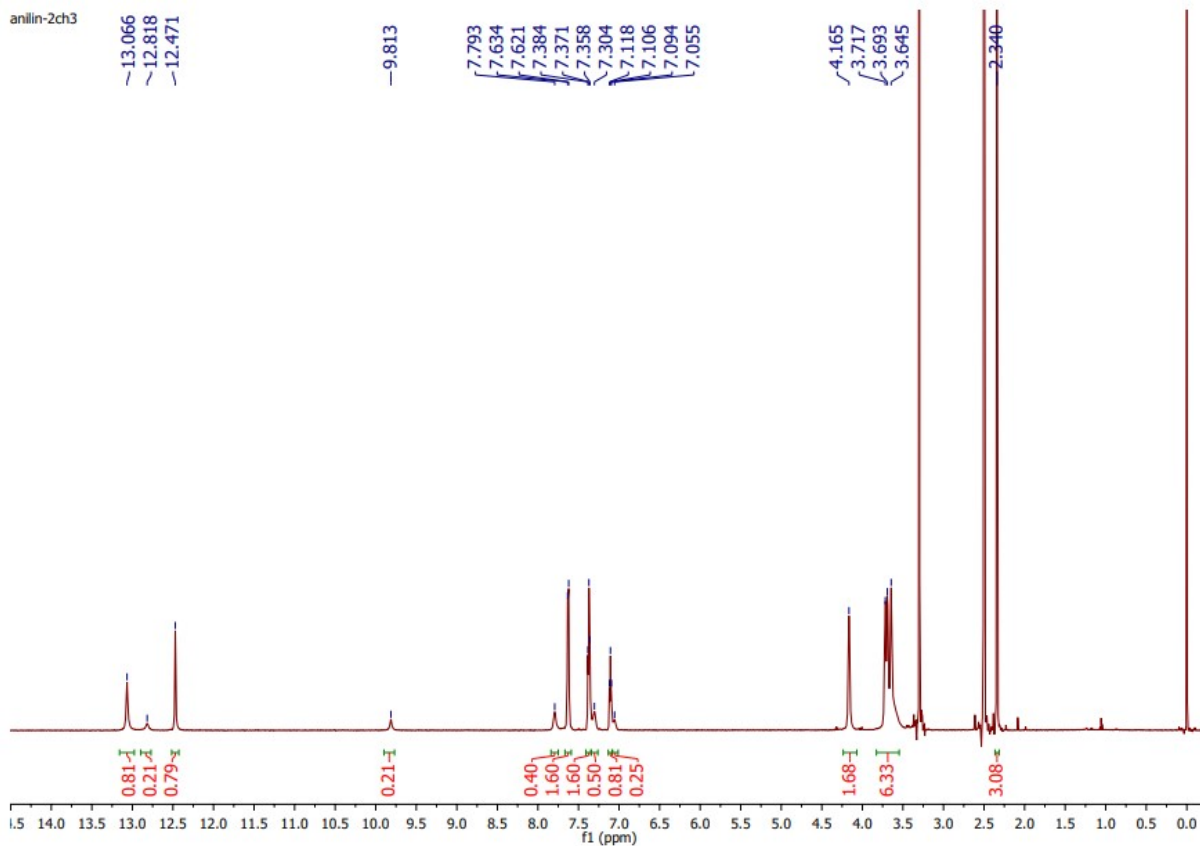
IR spectrum of compound 4d



IR spectrum of compound A1

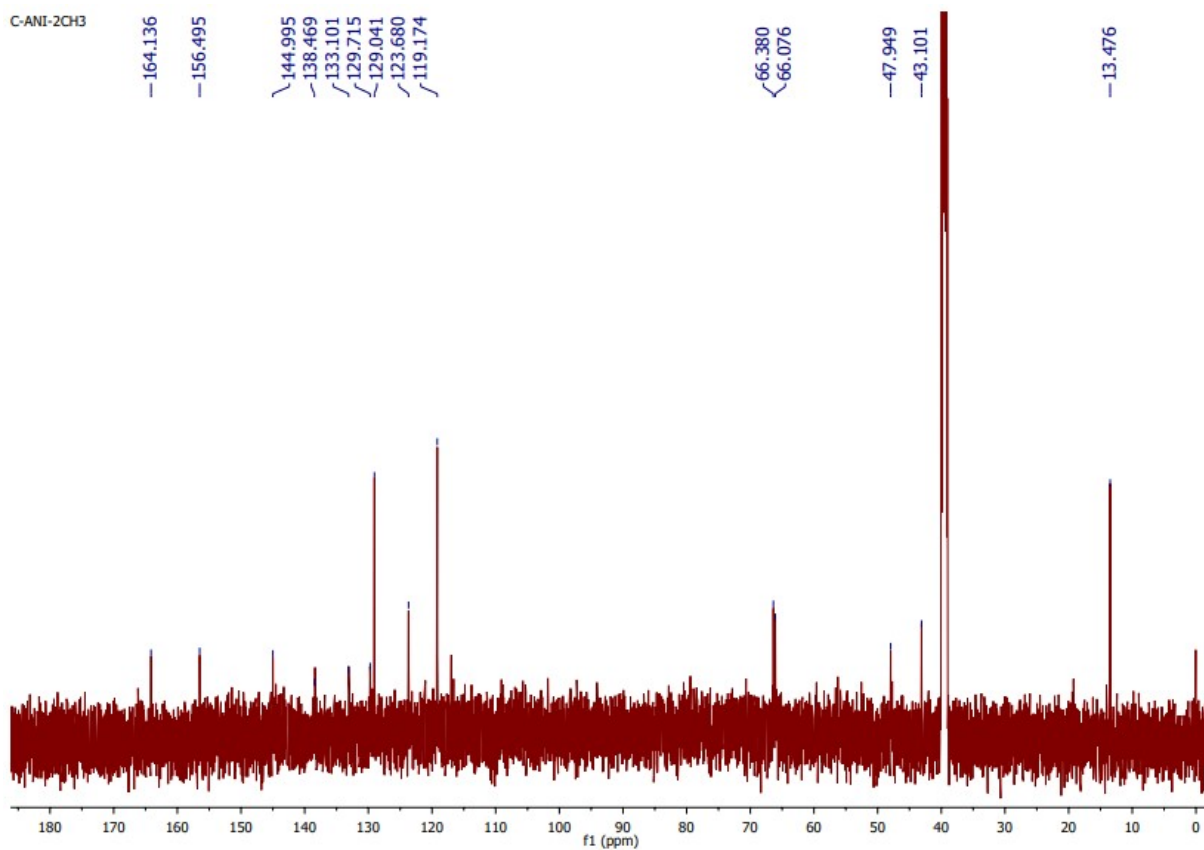


# Mass spectrum of compound A1

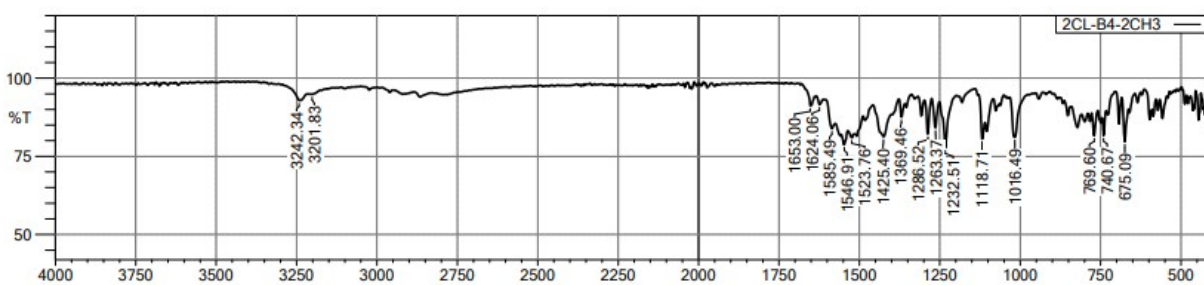




### <sup>1</sup>H-NMR of compound A1



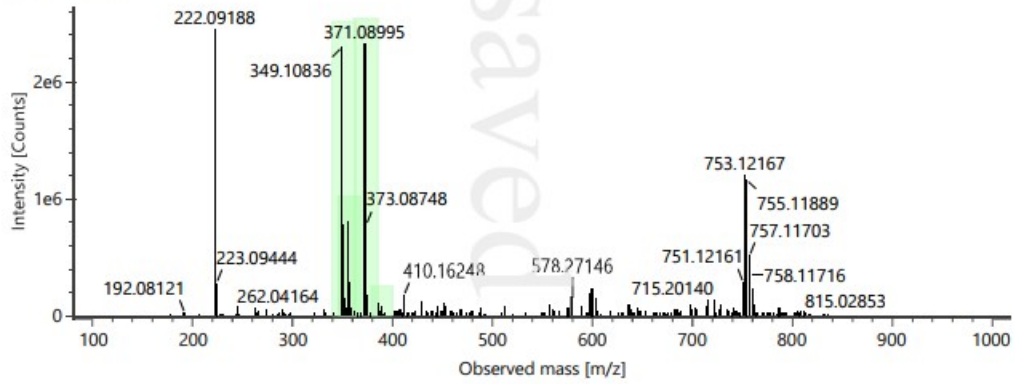
### <sup>13</sup>C-NMR of compound A1



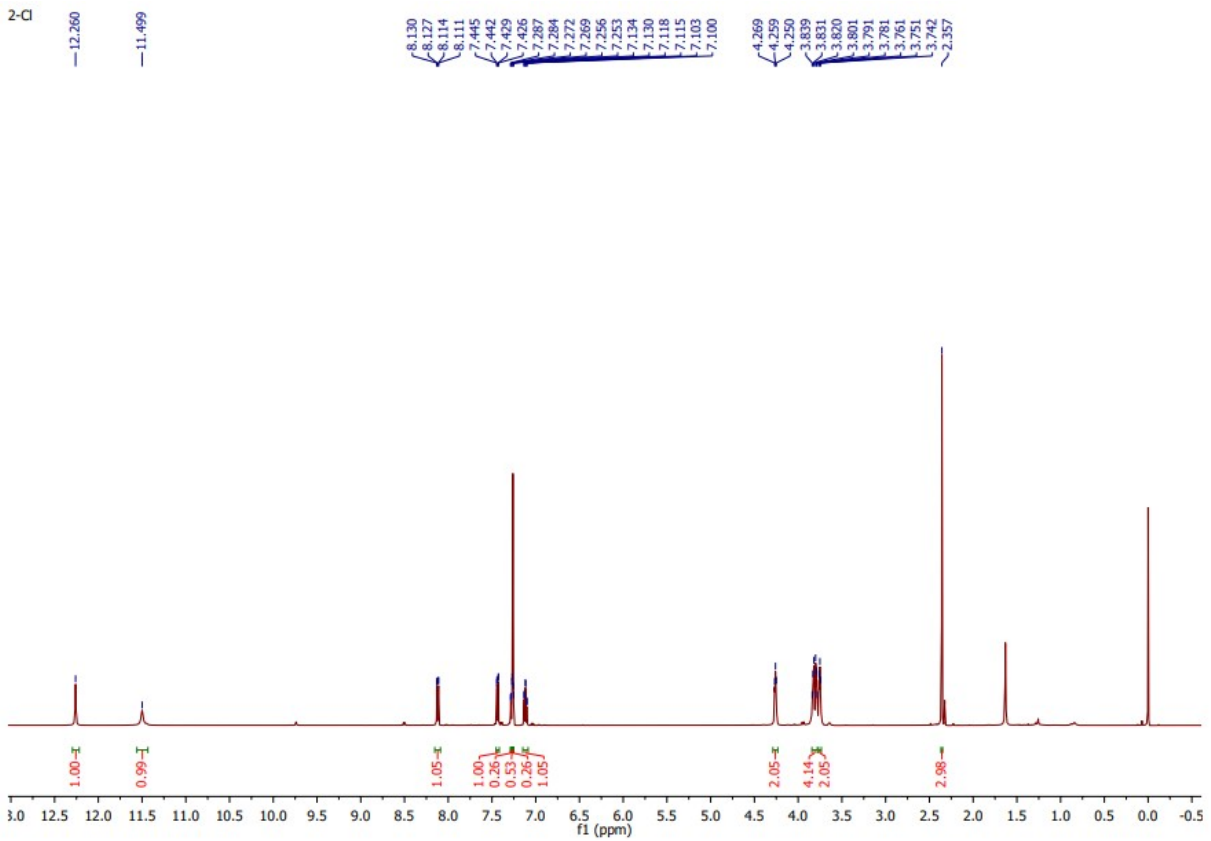
### IR spectrum of compound A2

Item name: Sample 3  
Item description:

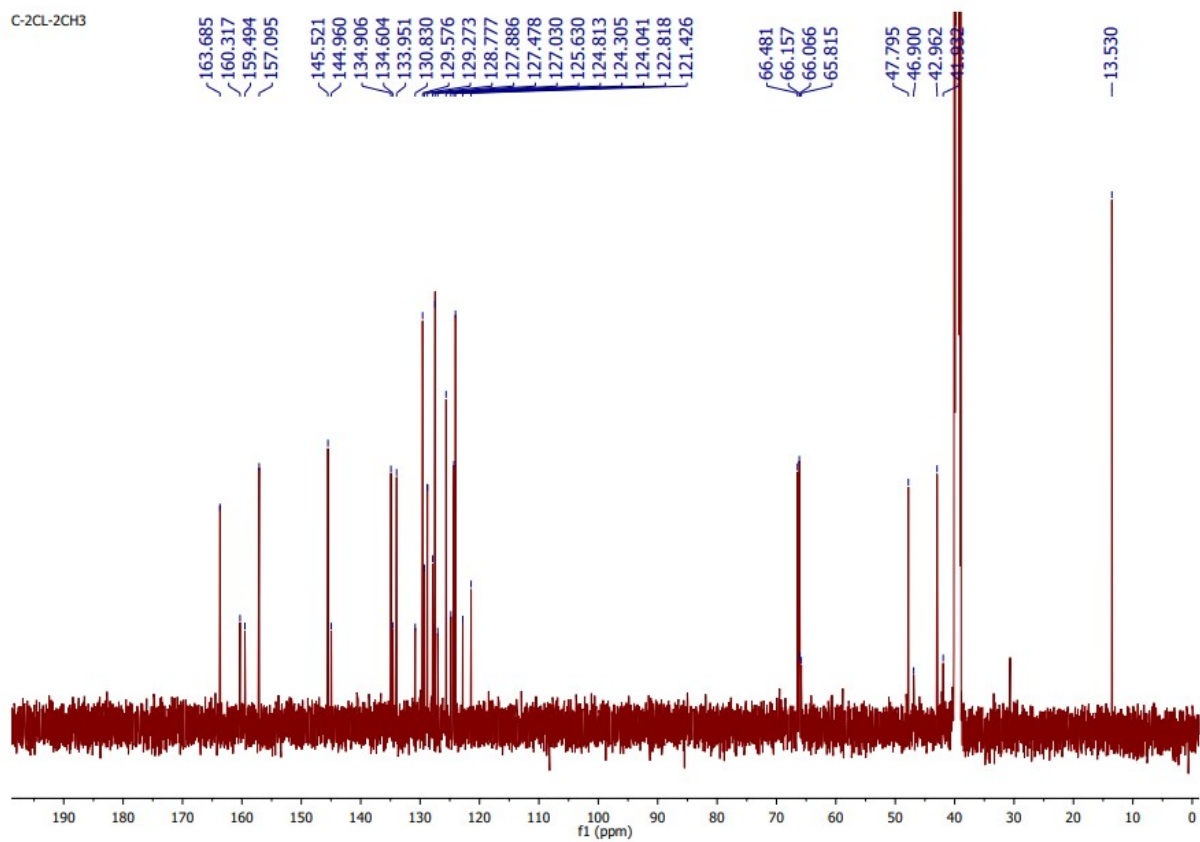
Channel name: Low energy : Time 5.1068 +/- 0.1421 minutes



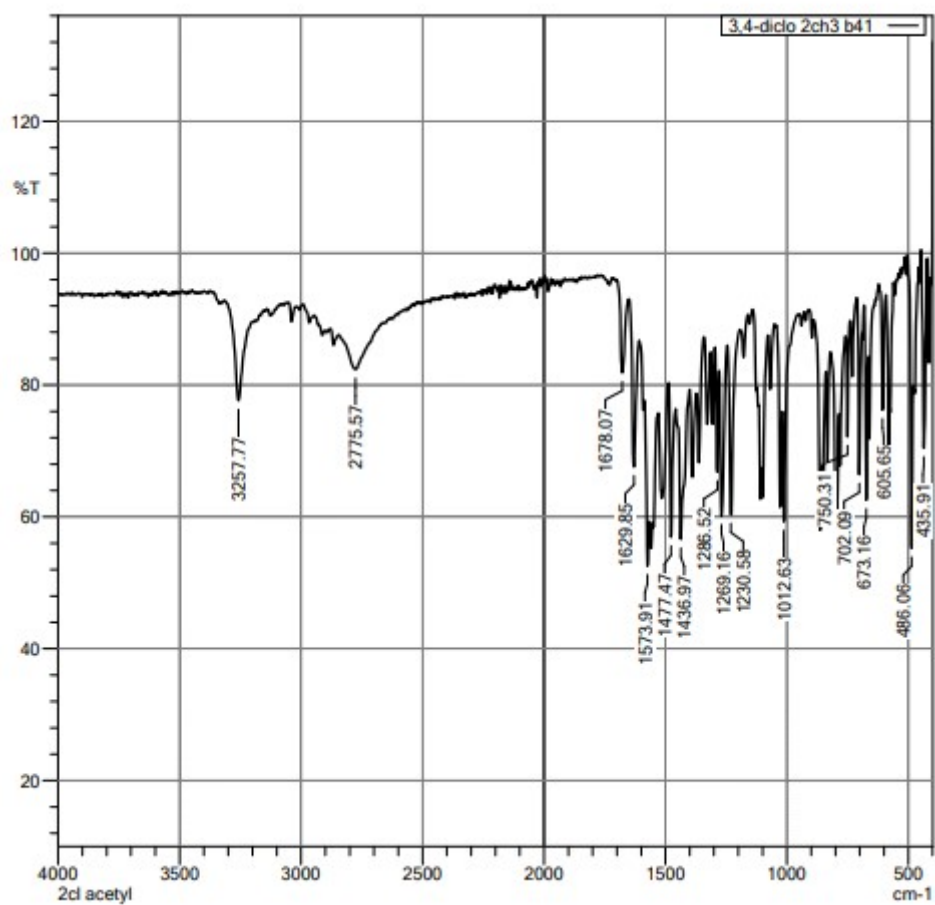
### Mass spectrum of compound A2



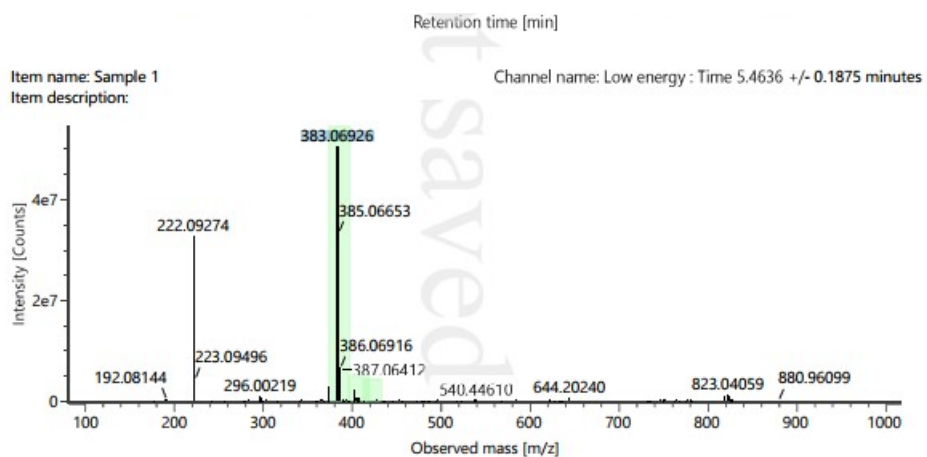
### <sup>1</sup>H-NMR spectrum of compound A2



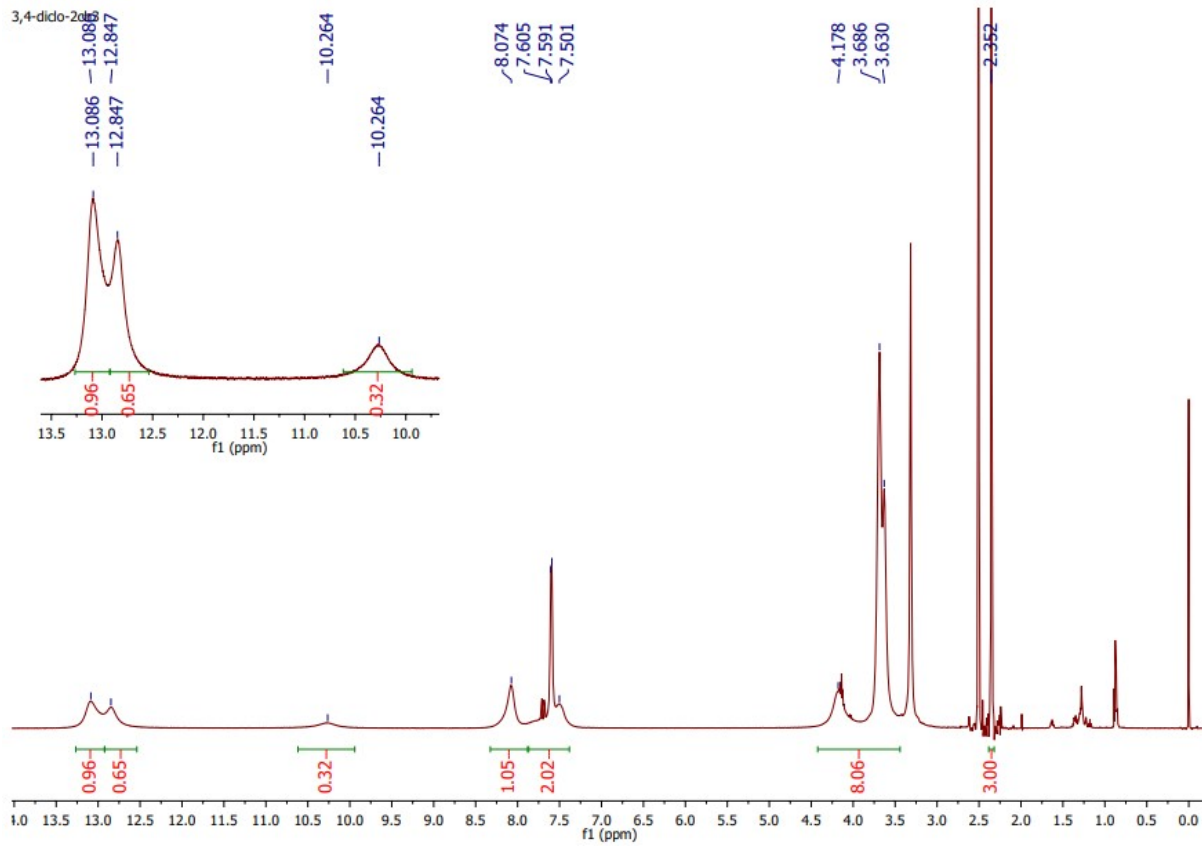
### <sup>13</sup>C-NMR spectrum of compound A2



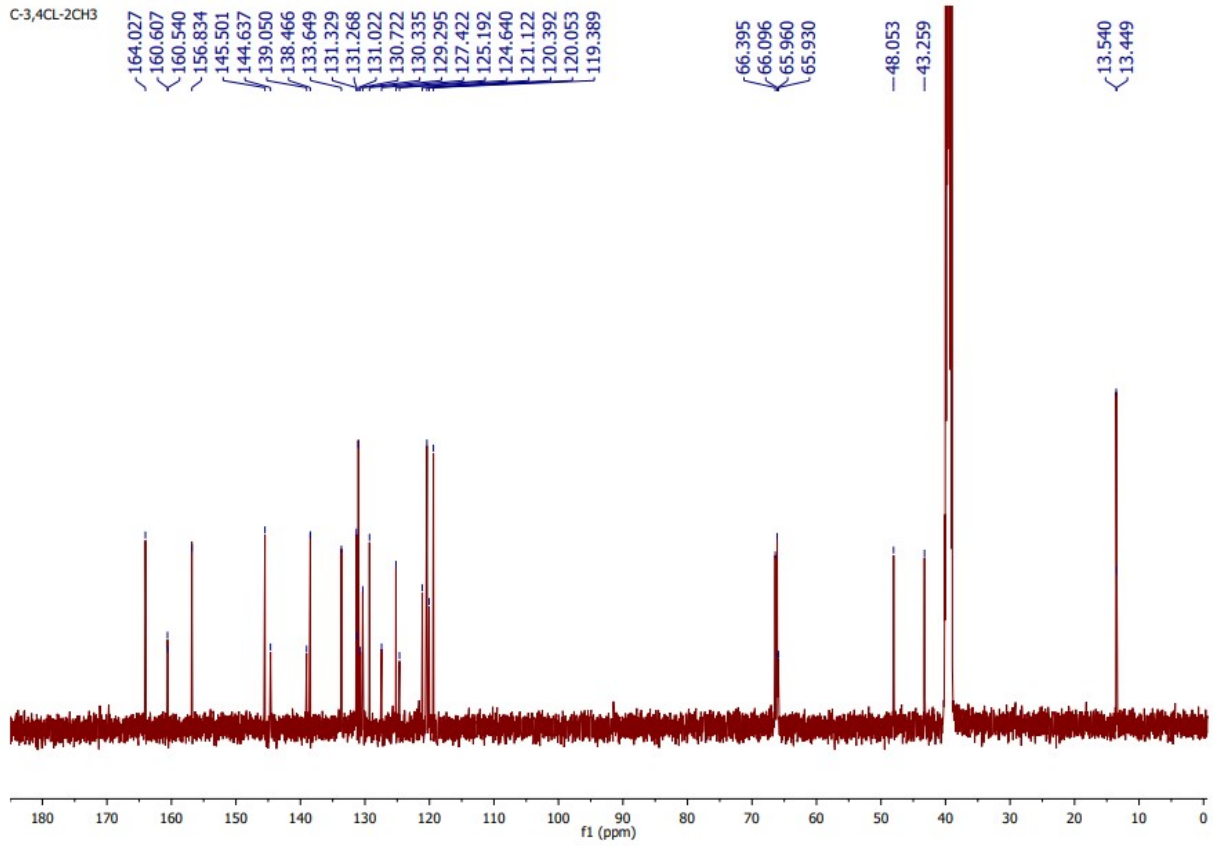
IR spectrum of compound A3



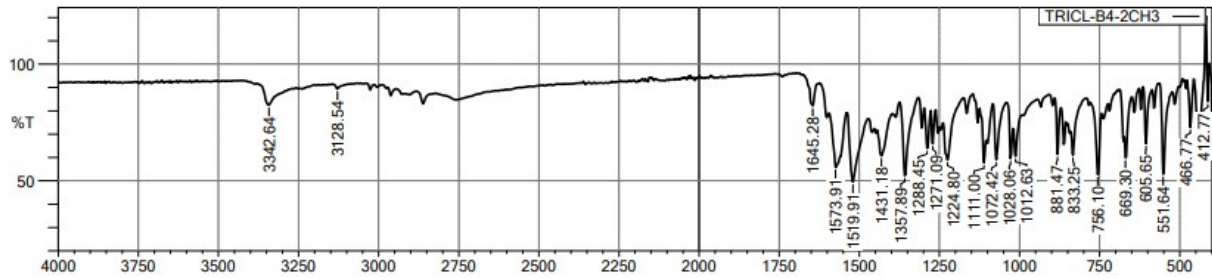
# Mass spectrum of compound A3



### <sup>1</sup>H-NMR of compound A3



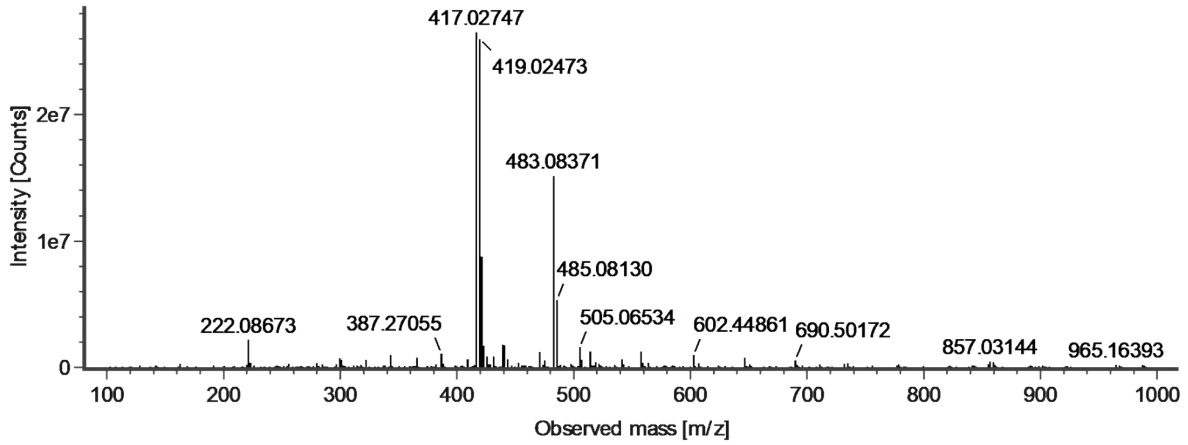
### <sup>13</sup>C-NMR of compound A3



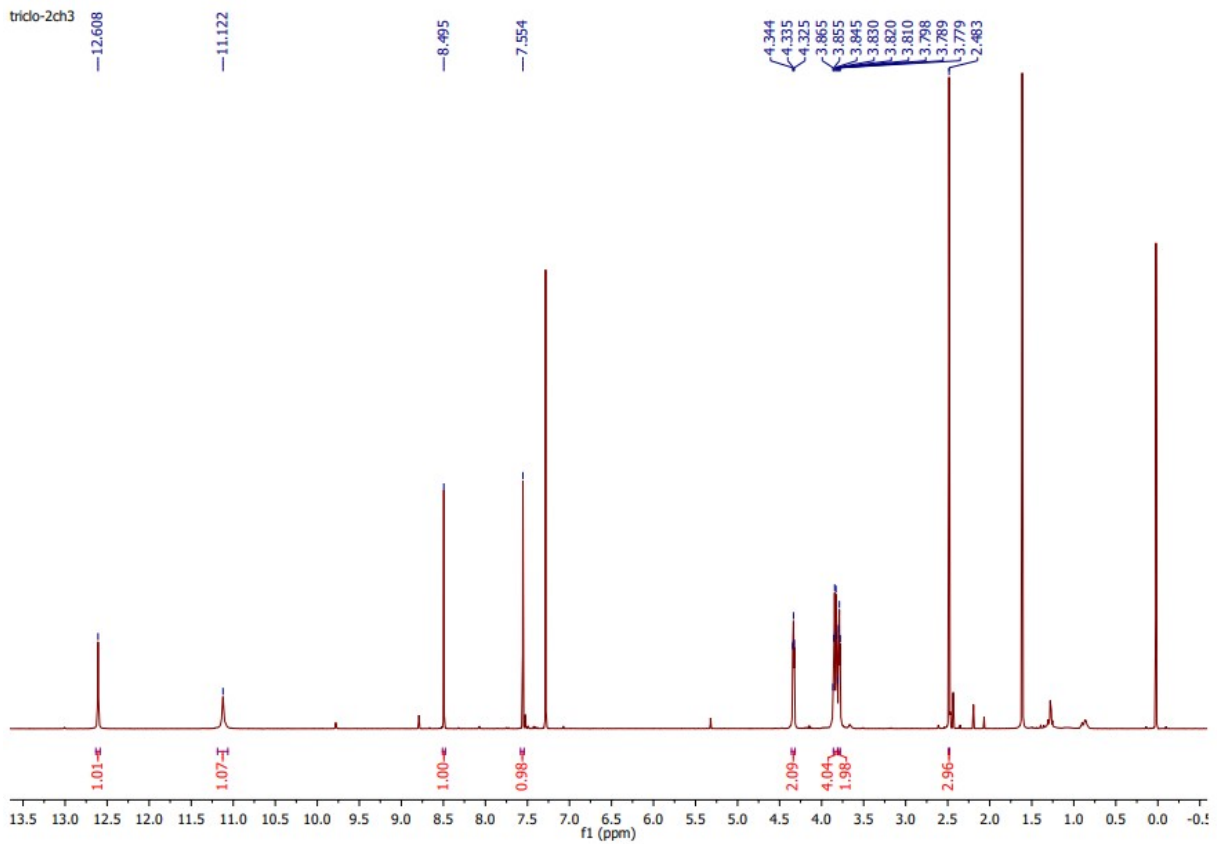
### IR spectrum of compound A4

Item name: B7  
Item description:

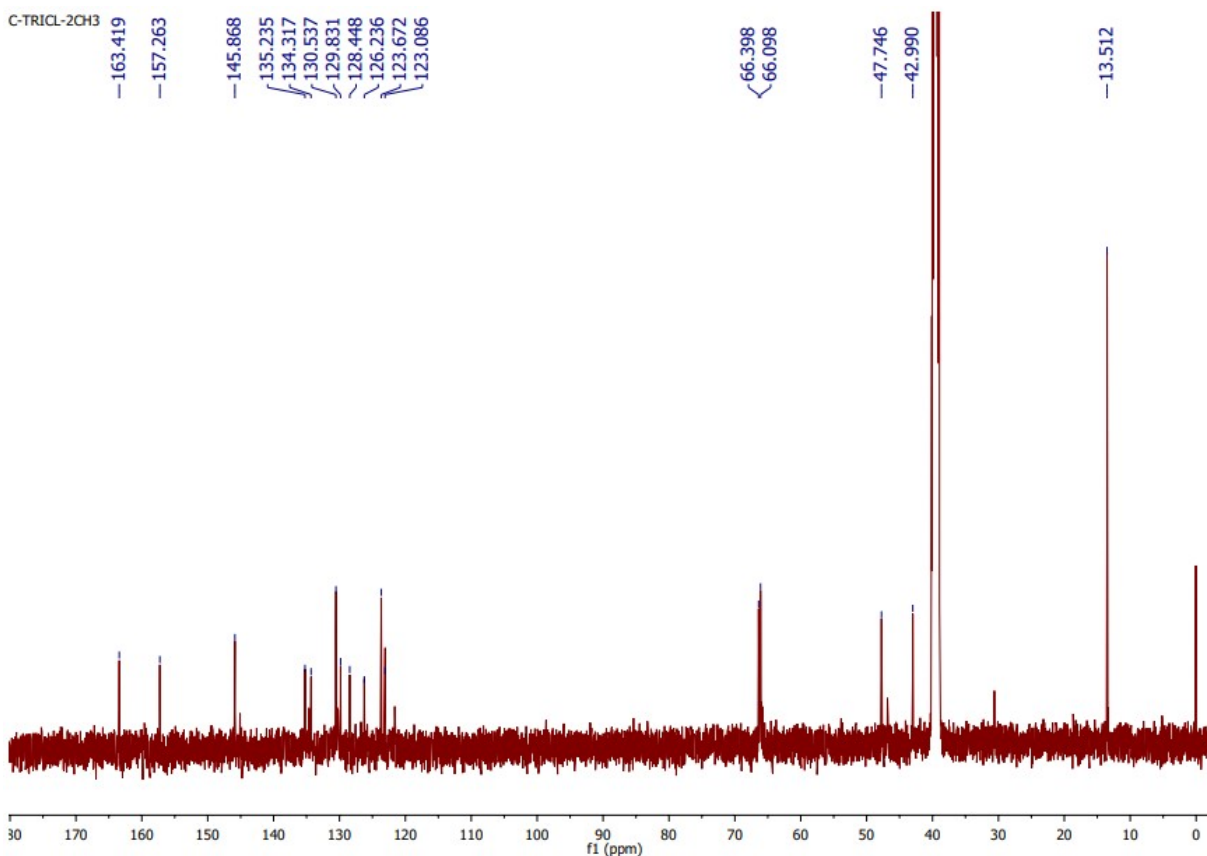
Channel name: Low energy : Time 7.5793 +/- 0.1007 minutes



### Mass spectrum of compound A4



## <sup>1</sup>H-NMR of compound A4



## <sup>13</sup>C-NMR of compound A4

### Author contributions

Thien-Vy Phan, MSC Pharm (Data curation: Equal; Formal analysis: Equal; Investigation: Lead; Validation: Equal; Visualization: Equal; Writing – original draft: Equal; Writing – review & editing: Equal); Phuong Nguyen Hoai Huynh, MSC Pharm (Data curation: Supporting; Formal analysis: Supporting; Investigation: Lead; Software: Supporting; Visualization: Equal; Writing – original draft: Supporting; Writing – review & editing: Supporting); Vu-Thuy-Vy Nguyen, Pharm (Data curation: Supporting; Formal analysis: Supporting; Investigation: Supporting; Software: Supporting; Visualization: Supporting); Thanh-Phuc Nguyen, Pharm (Formal analysis: Equal; Investigation: Supporting; Writing – original draft: Supporting); Thanh-Thao Vu, PhD Pharm (Data curation: Supporting; Methodology: Equal; Project administration: Supporting; Validation: Equal; Writing – original draft: Supporting); Cam-Van Thi Vo, PhD Pharm (Formal analysis: Supporting; Project administration: Supporting; Resources: Equal; Validation: Supporting; Writing – original draft: Supporting); Minh-Tri Le, PhD Pharm (Funding acquisition: Supporting; Investigation: Supporting; Project administration: Supporting; Resources: Supporting); Bao Gia Dang Nguyen, BSC (Data curation: Supporting; Formal analysis: Supporting; Investigation: Supporting; Writing – original draft: Supporting); Phuong Truong, PhD Pharm (Conceptualization: Equal; Funding acquisition: Supporting; Methodology: Equal; Supervision: Equal; Validation: Supporting; Writing – original draft: Supporting); Khac-Minh Thai, PhD Pharm (Conceptualization: Lead; Funding acquisition: Lead; Methodology: Lead; Project administration: Lead; Resources: Lead; Software: Lead; Supervision: Lead; Visualization: Equal; Writing – original draft: Lead; Writing – review & editing: Lead).



## References

1. Molecular operating environment (Version 2015.10), Chemical Computing Group ULC, Montreal, QC, Canada, 2016.
2. T.-V. Phan, V.-T.-V. Nguyen, C.-H.-H. Nguyen, T.-T. Vu, T.-D. Tran, M.-T. Le, D.-T. T. Trinh, V.-H. Tran and K.-M. Thai, *Journal of Biomolecular Structure and Dynamics*, 2023, 1-18.
3. Sybyl-X (Version 2.0), Certara, St. Louis, USA, 2011.
4. T.-D. Ngo, T.-D. Tran, M.-T. Le and K.-M. Thai, *Molecular diversity*, 2016, **20**, 945-961.
5. LeadIT (Version 2.0.2), BioSolveIT GmbH, Nordrhein-westfalen, Germany, 2012.
6. M.-T. Le, T. T. Mai, P. Huynh, T.-D. Tran, K.-M. Thai and Q.-T. Nguyen, *SAR and QSAR in Environmental Research*, 2020, **31**, 883-904.
7. M. J. Abraham, T. Murtola, R. Schulz, S. Páll, J. C. Smith, B. Hess and E. Lindahl, *SoftwareX*, 2015, **1**, 19-25.
8. Lindahl, Abraham, Hess, van der Spoel, GROMACS (Version 2020.6), Zenodo, Genève, Switzerland, 2021.
9. V. Zoete, M. A. Cuendet, A. Grosdidier and O. Michielin, *Journal of computational chemistry*, 2011, **32**, 2359-2368.
10. G. Bussi, D. Donadio and M. Parrinello, *The Journal of chemical physics*, 2007, **126**, 014101.
11. M. Parrinello and A. Rahman, *Journal of Applied physics*, 1981, **52**, 7182-7190.
12. B. Hess, H. Bekker, H. J. Berendsen and J. G. Fraaije, *Journal of computational chemistry*, 1997, **18**, 1463-1472.
13. T. T. Mai, P. G. Nguyen, M.-T. Le, T.-D. Tran, P. N. H. Huynh, D.-T. T. Trinh, Q.-T. Nguyen and K.-M. Thai, in *Mol Divers*, 2022, DOI: 10.1007/s11030-021-10359-4, pp. 1-20.
14. W. Humphrey, A. Dalke and K. Schulten, *Journal of molecular graphics*, 1996, **14**, 33-38.
15. C. C. David and D. J. Jacobs, in *Protein dynamics*, Springer, 2014, DOI: 10.1007/978-1-62703-658-0\_11, pp. 193-226.
16. The PyMOL Molecular Graphics System (Version 2.0), Schrödinger, LLC: New York, USA, 2017.
17. M. S. Valdés-Tresanco, M. E. Valdés-Tresanco, P. A. Valiente and E. Moreno, *Journal of Chemical Theory and Computation*, 2021, **17**, 6281-6291.
18. G. Xiong, Z. Wu, J. Yi, L. Fu, Z. Yang, C. Hsieh, M. Yin, X. Zeng, C. Wu and A. Lu, *Nucleic Acids Research*, 2021, **49**, W5-W14.
19. P. Kumar, K. Kadyan, M. Duhan, J. Sindhu, V. Singh and B. S. Saharan, *Chemistry Central Journal*, 2017, **11**, 1-14.
20. F. M. Vargas, *Journal of Chemical Education*, 2014, **91**, 396-401.
21. T. Baba, T. Ara, M. Hasegawa, Y. Takai, Y. Okumura, M. Baba, K. A. Datsenko, M. Tomita, B. L. Wanner and H. Mori, *Molecular systems biology*, 2006, **2**, 2006.0008.
22. C. H. Teh, W. A. Nazni, A. H. Nurulhusna, A. Norazah and H. L. Lee, *BMC microbiology*, 2017, **17**, 1-8.
23. M. N. Gallucci, M. Oliva, C. Casero, J. Dambolena, A. Luna, J. Zygodlo and M. Demo, *Flavour and fragrance journal*, 2009, **24**, 348-354.
24. K. E. Whalen, K. L. Poulson-Ellestad, R. W. Deering, D. C. Rowley and T. J. Mincer, *Journal of natural products*, 2015, **78**, 402-412.
25. T. J. Opperman, S. M. Kwasny, H.-S. Kim, S. T. Nguyen, C. Houseweart, S. D'Souza, G. C. Walker, N. P. Peet, H. Nikaido and T. L. Bowlin, *Antimicrobial agents and chemotherapy*, 2014, **58**, 722-733.